A Lightweight Multimode Medical Image Fusion Method Using Similarity Measure Between Intuitionistic Fuzzy Sets Joint Laplacian Pyramid

Qian Jiang, Xin Jin, *Member, IEEE*, Xiaohui Cui, Shaowen Yao, *Member, IEEE*, Keqin Li, *Fellow, IEEE*, and Wei Zhou, *Member, IEEE*

***Abstract*—Medical image fusion combines the multiple features of human tissue from different source images, which will be conducive to clinical diagnosis. Because of the human visual perception and mechanisms of medical imaging, abundant fuzzy features exist in medical image fusion with remarkable influence. To address this issue, we introduce the similarity measure of fuzzy set theory into medical image fusion to abstract and measure these fuzzy features. In this study, we present a new similarity measure of intuitionistic fuzzy set theory to represent image features and present a lightweight medical image fusion technique on the basis of this new measure. First, the new similarity measure is proposed according to geometric modeling technique and verified by mathematical justification. Second, a set of high frequency sub-images and a low frequency sub-image are produced by Laplacian pyramid decomposition to separate different image features. Third, our proposed similarity measure is utilized to describe and extract the detailed image features. Finally, two fusion rules and inverse Laplacian pyramid decomposition are sequentially used to get the fused image. This research shows that the similarity measure of fuzzy set theory can get excellent performance in medical image fusion. Experiments reveal that our similarity measure and medical image fusion method both have the superior performance to most of the existing methods.**

***Index Terms*—Feature extraction, fuzzy sets, Laplacian pyramid, image processing, information fusion, medical image fusion.**

Manuscript received 2 April 2022; revised 18 November 2022; accepted 13 December 2022. Date of publication 14 February 2023; date of current version 25 May 2023. This work was supported in part by the National Natural Science Foundation of China under Grants 62101481, 62002313, 62261060, 62166047, 62162067, and 62101480, in part by the Basic Research Project of Yunnan Province under Grants 202201AU070033, 202201AT070112, 202001BB050076, 202201AU070034, and 202201AT070173, in part by Major Scientific and Technological Project of Yunnan Province under Grant 202202AD080002, and in part by Key Laboratory in Software Engineering of Yunnan Province under Grant 2020SE408. *(Corresponding authors: Xin Jin; Xiaohui Cui.)*

Qian Jiang, Xin Jin, Shaowen Yao, and Wei Zhou are with the Engineering Research Center of Cyberspace, Yunnan University, Kunming, Yunnan 650091, China, and also with the School of Software, Yunnan University, Kunming 650091, China (e-mail: jiangqian_1221@163.com; xinxin_jin@163.com; yaosw@ynu.edu.cn; zwei@ynu.edu.cn).

Xiaohui Cui is with the School of Cyber Science and Engineering, Wuhan University, Wuhan 430000, China (e-mail: xcui@whu.edu.cn).

Keqin Li is with the Department of Computer Science, State University of New York, New Paltz, NY 12561 USA (e-mail: lik@newpaltz.edu).

The code is available at https://github.com/jinxinhuo/SMIFS.

This article has supplementary downloadable material available at https://doi.org/10.1109/TETCI.2022.3231657, provided by the authors.

Digital Object Identifier 10.1109/TETCI.2022.3231657

I. Introduction

A. Motivation

THE cognition and judgment of human for the real world are often characterized by non-quantitative fuzziness, that is, the description of physical objects in the real world is usually imprecise and uncertain [1], [2], [3]. Therefore, a mass of vague and uncertain information (or features) exists in the field of computer science when it is used for practical applications. These fuzzy features are usually difficult to be processed with conventional techniques, but they are helpful for pattern recognition or classification [1], [4], [6]. To effectively address this problem, Zadeh [1] established fuzzy set (FS) theory in 1965. Because of the excellent capacity, FS theory provides a powerful mathematical tool for addressing the fuzzy and uncertain problems in various fields, such as information fusion, image processing, and automatic control [2], [3], [5], [6].

Considering the limited descriptive power of conventional FS theory [1], scholars have introduced some enhanced theory based on conventional FS to further improve the performance for dealing with fuzzy features, such as type-2 fuzzy set (T2FS) [7], [8] and intuitionistic fuzzy set (IFS) [9]. Moreover, the information measurement of fuzzy sets is one of the most significant techniques, including entropy, similarity, and distance measure [10], [11]. Among them, similarity and distance measures are two relative concepts in fuzzy theory, and they can effectively measure or quantify the similarity or difference between two different fuzzy sets and are widely used in pattern recognition and classification, clustering analysis, decision making, and feature extraction [11], [12], [13]. Many scholars have devoted themselves in this field and proposed a series of fuzzy measurement models [12], [13], [14]. However, most of the existing measures still have shortcomings that may lead to some unreasonable or incorrect decisions in their applications. Thus, more explorations are wanted to improve the performances of fuzzy measures, and the extensions of these measures for the real applications are also expected.

Medical image fusion is a challenging problem with abundant fuzzy features in information fusion [15], and it is usually used to fuse the complementary information of computed tomography (CT) and magnetic resonance imaging (MRI), which are obtained by the corresponding sensors [16], [17]. Therefore, medical image fusion can be employed to overcome the limitation of information description in single sensor images that are related to the acquisition equipment or physical conditions. Generally, there exists a mass of fuzzy features in image fusion, and the fuzziness mainly comes from two points: first, the information loss of the imaging process will generate some fuzzy and uncertainty features; second, the fuzzy and uncertainty of human visual perception for the visual information [17]. Besides, it is a significant factor for medical image fusion to get the pixel weight that should be related to the features of pixel value and its neighboring pixels, which can be regarded as a fuzzy and uncertainty problem. Thus, the feature presentation of FS theory is expected to enhance the fusion performance of medical images [21], [22]. Besides, it is necessary and reasonable to introduce some novel techniques based on fuzzy theory to measure the features of medical images because of the ability for addressing the imprecise and uncertain information.

Generally, medical image fusion methods are considered as two strategies: transform domain and spatial domain methods [15], [16], [17], [18]. Conventional spatial domain-based methods usually have the advantage of fast speed and smaller memory, but the performance is usually inferior to the transform domain-based methods due to the limited feature representation ability. Besides, the popular deep learning method is generally treated as the spatial domain-based technique, and most deep learning models require a mass of training samples with excessive running time and memory space [18], [19]. However, it is a difficult problem to get enough training samples in this field. Transform domain-based image fusion methods usually include three steps: image transform or image decomposition, sub-band images or coefficients fusion, and inverse transform or image reconstruction. Transform domain-based methods are the most popular techniques in medical image fusion, which are benefit by the stable feature representation ability, but the fuzziness or uncertainty of medical image features is not often well-handled in conventional methods. In addition, most medical image fusion methods tend to be more complex for producing competitive fused images, which leads to an increase in running time and computing resources. Therefore, it is necessary to explore some lightweight and effective medical image fusion methods, as well as the feature representation method based on the measure of FS theory.

B. Our Contributions

According to the above analysis, the performance of similarity measure between FSs should be improved for its real applications, and the lightweight or easily implemented method of medical image fusion is significant for clinical diagnosis. Therefore, this work combines the theoretical result with the real application to propose a lightweight medical image fusion method via the feature measurement of IFSs. The contributions of our work are summarized as follows:

1) We propose a new similarity measure of IFS theory based on geometric modeling technique that is accessible and superior compared with the most of existing methods.
2) We introduce the new proposed similarity measure between IFSs into the feature presentation of medical images, which is a combination of fuzzy theoretical study and practical application.
3) We design an effective and lightweight medical image fusion technique by introducing the new proposed similarity measure between IFSs, which has outstanding performance in at medical image fusion, as well as the simple structure and fast processing speed.

The remainder contents are presented as follows. Section II reports the basic knowledge. Section III presents the new similarity measure and its corresponding theoretical proof, as well as the our new method. Section IV shows the numerical experiments and the applications of the reported measure theory for medical image fusion. Section V concludes this work.

II. Preliminaries

To effectively deal with the vague or imprecise information in the real world, Zadeh proposed FS theory [1], which utilizes membership function to present the fuzzy features [6]. FS theory makes up the deficiency of conventional set theory and lays the foundation for the development of fuzzy theory. In 1986, IFS theory [9], [20] was proposed by reintroducing hesitation in the conventional FS theory, which further improves the ability to describe uncertain information. Besides, the similarity measure is also a hot topic in FS to measure the similarity between two FS [21], [22].

A. Intuitionistic Fuzzy Sets

There are three feature parameters as membership, nonmembership, and hesitancy in IFS theory, and the definitions and properties are introduced as below.

Definition 1: Given a domain of discourse $X = \{x_1, x_2, \ldots, x_n\}$, the definition of IFS A is:

$$A = \{\langle x, \mu_A(x), \nu_A(x)\rangle \,|x \in X\},$$

where $\mu_A(x)$ is the membership, and $\nu_A(x)$ is the nonmembership. The hesitancy function $\pi_A(x)$ satisfies the constraint conditions with $\pi_A(x) = 1 - \mu_A(x) - \nu_A(x)$; and $\mu_A(x)$, $\nu_A(x)$, and $\pi_A(x)$ are all fall into the value ranges of [0, 1]. What's more, the IFS can be translated into the conventional FS, when $\pi_A(x) = 0$.

Atanassov and Gargov [23] revealed that the IFS has an equipollent extension of FS as interval-valued fuzzy set (IVFS) which has a mapping relation with IFS. For example, given a IVFS $B = \{\langle x, \mu_{BL}(x), \mu_{BT}(x)\rangle \,|x \in X\}$ with $0 \leq \mu_{BL}(x) \leq \mu_{BT}(x) \leq 1$, and the map f which assigns to every IVFS B with an IFS A: $B = f(A)$, given by $\mu_{BL}(x) = \mu_A(x)$

and $\mu_{BT}(x) = 1 - \nu_A(x)$. The mapping is the same in reverse, the properties in IFSs are therefore adapted to IVFSs as well.

Definition 2: The fuzzy operations between two IFSs *A* and *B* are described as follows [24]:

1) If $A \subseteq B$, then $\mu_A(x) \leq \mu_B(x)$, $\nu_A(x) \geq \nu_B(x)$;
2) If $A = B$, then $\mu_A(x) = \mu_B(x)$, $\nu_A(x) = \nu_B(x)$.

B. Similarity Measure Between Intuitionistic Fuzzy Sets

Similarity measure describes the similarity (or difference) degree between two IFSs, which is an important indicators in IFS theory [10], [11]. The definition of similarity measure between IFSs can be presented by Definition 3.

Definition 3: The similarity measure between two different IFSs *A* and *B* must satisfy five established **Properties** [25], [26], [27], as follows:

1) $0 \leq s(A,B) \leq 1$;
2) $s(A,B) = 1$ if and only if $A = B$;
3) $s(A,B) = s(B,A)$;
4) if $A \subseteq B \subseteq C$, then $s(A,C) \leq s(A,B)$ and $s(A,C) \leq s(B,C)$;
5) if A is a crisp set, then $s(A, A^C) = 0$.

III. Our Proposed Method

This section reports our proposed similarity measure and lightweight medical image fusion method. First, the new similarity measure of IFSs is introduced via geometric modeling method which is built by the fuzzy numbers of transformed symmetrical triangle from the feature parameters of IFSs, and the new measure is verified by Definition 3 to prove its rationality. Second, an effective and lightweight medical image fusion scheme is designed with the combination of Laplacian pyramid decomposition (LPD) and the proposed similarity theory which is applied to measure the vague and imprecise features in the source medical images.

A. Our Proposed Similarity Measure Between IFSs

In IFS theory, similarity measure is a significant theoretical model because of its excellent ability for presenting the vague or uncertain features in information science. And the effectiveness of similarity measure will have seriously influence on the reasonability of decisions. The shortcomings of the existing measures can be classified into two situations: one is that some measures are unable to make decisions in some specific cases, and other measures may give unreasonable decisions. Therefore, a more effective similarity measure is proposed to improve the performance of IFSs. First, the different forms of IFS are given as Definition 4.

Definition 4: A given IFS *A* in the universe of discourse $X = \{x_1, x_2, \ldots, x_n\}$ can be converted to IVFS, which is expressed as follows:

$$A = \{\langle x, \mu_A(x), 1-\nu_A(x)\rangle \,|x \in X\}.$$

For simplicity, the fuzzy numbers of transformed IVFS A are described as below:

$$A_T = \{\langle x, T_{\mu_A}(x), T_{\nu_A}(x)\rangle \,|x \in X\},$$

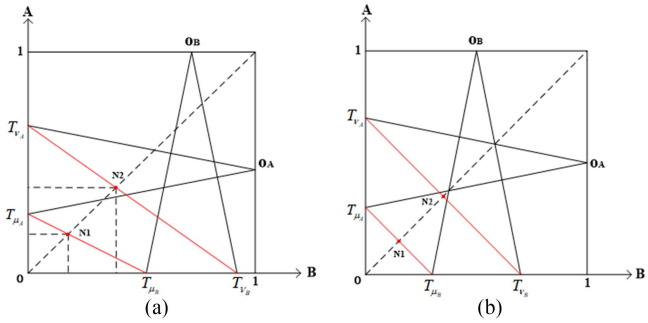

Fig. 1. Transformed equilateral triangles of IFSs *A* and *B*. (a) Example 1; (b) Example 2 .

where the fuzzy number $T_{\mu_A}(x)$ is another form of feature parameter $\mu_A(x)$, and the fuzzy number $T_{\nu_A}(x)$ is another form of the $1-\nu_A(x)$.

When calculate the distance or similarity between two IFSs A and B, we put the transformed fuzzy numbers of IFSs A and B on different coordinate axis respectively, and the corresponding transformed isosceles triangles are built according to transformed fuzzy numbers, and then the measure can be constructed based on these transformed isosceles triangles by the distances between some specific points. Fig. 1 shows the transformed geometric model of two different IFSs which are set up on the corresponding axes (x or y). Geometric model-based modeling method is intuitive and easy to understand. Fig. 1(a) is the situation that IFS *A* is different from IFS *B*, and the situation of IFSs $A = B$ is shown as Fig. 1(b). O_A and O_B are respectively the transformed triangle vertex of IFSs A and B. N_1 and N_2 are respectively the intersection of $\overline{T_{\mu_A}T_{\mu_B}} = -T_{\mu_A}x/T_{\mu_B} + T_{\mu_A}$ and $\overline{T_{\nu_A}T_{\nu_B}} = -T_{\nu_A}x/T_{\nu_B} + T_{\nu_A}$ with the diagonal line. Our proposed similarity measure is related to the sum of two specific line segments: one is the length difference between $\overline{T_{\mu_A}N_1}$ and $\overline{T_{\mu_B}N_1}$, and another is the length difference value between $\overline{T_{\nu_A}N_2}$ and $\overline{T_{\nu_B}N_2}$. Therefore, the coordinates of N_1 and N_2 should be calculated firstly, and the operation is shown as follows.

The X-axes of N_1 is presented as:

$$N_{1\overline{T_{\mu_A}T_{\mu_B}}} = N_{1\overline{y=x}},$$
$$\Rightarrow -T_{\mu_A}N_{1x}/T_{\mu_B} + T_{\mu_A} = N_{1x},$$
$$\Rightarrow N_{1x} = T_{\mu_A}T_{\mu_B}/(T_{\mu_B} + T_{\mu_A}),$$

then, we can get the Y-axes of N_1 as:

$$N_{1y} = N_{1x} = T_{\mu_A}T_{\mu_B}/(T_{\mu_B} + T_{\mu_A}).$$

Besides, the X-axes of N_2 is presented as:

$$N_{2\overline{T_{\nu_A}T_{\nu_B}}} = N_{2\overline{y=x}},$$
$$\Rightarrow -T_{\nu_A}N_{2x}/T_{\nu_B} + T_{\nu_A} = N_{2x},$$
$$\Rightarrow N_{2x} = T_{\nu_A}T_{\nu_B}/(T_{\nu_B} + T_{\nu_A}),$$

then, the Y-axes of N_2 is presented as:

$$N_{2y} = N_{2x} = T_{\nu_A}T_{\nu_B}/(T_{\nu_B} + T_{\nu_A}).$$

As a result, the $\overline{T_{\mu_A}N_1}$ and $\overline{T_{\mu_B}N_1}$ can be calculated according to the coordinate of N_1 as:

$$\begin{aligned}
\overline{T_{\mu_A}N_1} &= \sqrt{\overline{T_{\mu_A}N_{1y}}^2 + \overline{N_{1y}N_1}^2} \\
&= \sqrt{(T_{\mu_A} - N_{1y})^2 + (N_1 - N_{1y})^2} \\
&= \sqrt{\left(T_{\mu_A} - \frac{T_{\mu_A}T_{\mu_B}}{T_{\mu_B}+T_{\mu_A}}\right)^2 + \left(\frac{T_{\mu_A}T_{\mu_B}}{T_{\mu_B}+T_{\mu_A}}\right)^2} \\
&= \sqrt{\left(\frac{T_{\mu_A}T_{\mu_B}+{T_{\mu_A}}^2}{T_{\mu_B}+T_{\mu_A}} - \frac{T_{\mu_A}T_{\mu_B}}{T_{\mu_B}+T_{\mu_A}}\right)^2 + \left(\frac{T_{\mu_A}T_{\mu_B}}{T_{\mu_B}+T_{\mu_A}}\right)^2} \\
&= \sqrt{\left(\frac{{T_{\mu_A}}^2}{T_{\mu_B}+T_{\mu_A}}\right)^2 + \left(\frac{T_{\mu_A}T_{\mu_B}}{T_{\mu_B}+T_{\mu_A}}\right)^2} \\
&= \sqrt{\frac{{T_{\mu_A}}^2({T_{\mu_A}}^2+{T_{\mu_B}}^2)}{(T_{\mu_B}+T_{\mu_A})^2}} \\
&= \frac{T_{\mu_A}\sqrt{{T_{\mu_A}}^2+{T_{\mu_B}}^2}}{T_{\mu_B}+T_{\mu_A}}, \\
\overline{T_{\mu_B}N_1} &= \sqrt{\overline{N_{1x}T_{\mu_B}}^2 + \overline{N_{1x}N_1}^2} \\
&= \sqrt{(T_{\mu_B} - N_{1x})^2 + (N_1 - N_{1x})^2} \\
&= \sqrt{\left(T_{\mu_B} - \frac{T_{\mu_A}T_{\mu_B}}{T_{\mu_B}+T_{\mu_A}}\right)^2 + \left(\frac{T_{\mu_A}T_{\mu_B}}{T_{\mu_B}+T_{\mu_A}}\right)^2} \\
&= \sqrt{\left(\frac{{T_{\mu_B}}^2+T_{\mu_A}T_{\mu_B}}{T_{\mu_B}+T_{\mu_A}} - \frac{T_{\mu_A}T_{\mu_B}}{T_{\mu_B}+T_{\mu_A}}\right)^2 + \left(\frac{T_{\mu_A}T_{\mu_B}}{T_{\mu_B}+T_{\mu_A}}\right)^2} \\
&= \sqrt{\left(\frac{{T_{\mu_B}}^2}{T_{\mu_B}+T_{\mu_A}}\right)^2 + \left(\frac{T_{\mu_A}T_{\mu_B}}{T_{\mu_B}+T_{\mu_A}}\right)^2} \\
&= \sqrt{\frac{{T_{\mu_B}}^2({T_{\mu_A}}^2+{T_{\mu_B}}^2)}{(T_{\mu_B}+T_{\mu_A})^2}} \\
&= \frac{T_{\mu_B}\sqrt{{T_{\mu_A}}^2+{T_{\mu_B}}^2}}{T_{\mu_B}+T_{\mu_A}}.
\end{aligned}$$

Then, the length difference value between $\overline{T_{\mu_A}N_1}$ and $\overline{T_{\mu_B}N_1}$ can be get as:

$$\begin{aligned}
d_1 &= \left|\overline{T_{\mu_B}N_1} - \overline{T_{\mu_A}N_1}\right| \\
&= \left|\frac{T_{\mu_B}\sqrt{{T_{\mu_A}}^2+{T_{\mu_B}}^2}}{T_{\mu_B}+T_{\mu_A}} - \frac{T_{\mu_A}\sqrt{{T_{\mu_A}}^2+{T_{\mu_B}}^2}}{T_{\mu_B}+T_{\mu_A}}\right| \\
&= \left|\frac{(T_{\mu_B}-T_{\mu_A})\sqrt{{T_{\mu_A}}^2+{T_{\mu_B}}^2}}{T_{\mu_B}+T_{\mu_A}}\right|.
\end{aligned}$$

By the same derivation, the length difference value between $\overline{T_{\nu_A}N_2}$ and $\overline{T_{\nu_B}N_2}$ can be got as:

$$\begin{aligned}
d_2 &= \left|\overline{T_{\nu_B}N_2} - \overline{T_{\nu_A}N_2}\right| \\
&= \left|\frac{T_{\nu_B}\sqrt{{T_{\nu_A}}^2+{T_{\nu_B}}^2}}{T_{\nu_B}+T_{\nu_A}} - \frac{T_{\nu_A}\sqrt{{T_{\nu_A}}^2+{T_{\nu_B}}^2}}{T_{\nu_B}+T_{\nu_A}}\right| \\
&= \left|\frac{(T_{\nu_B}-T_{\nu_A})\sqrt{{T_{\nu_A}}^2+{T_{\nu_B}}^2}}{T_{\nu_B}+T_{\nu_A}}\right|.
\end{aligned}$$

Therefore, the distance between IFSs A and B is presented as (1):

$$\begin{aligned}
d &= \frac{1}{2}(d_1+d_2) \\
&= \frac{1}{2}\left[\left|\frac{(T_{\mu_B}-T_{\mu_A})\sqrt{{T_{\mu_A}}^2+T_{\mu_B}{}^2}}{T_{\mu_B}+T_{\mu_A}}\right| + \left|\frac{(T_{\nu_B}-T_{\nu_A})\sqrt{{T_{\nu_A}}^2+{T_{\nu_B}}^2}}{T_{\nu_B}+T_{\nu_A}}\right|\right] \\
&= \frac{1}{2}\left[\left|\frac{(\mu_B-\mu_A)\sqrt{{\mu_A}^2+{\mu_B}^2}}{\mu_B+\mu_A}\right| + \left|\frac{(\nu_A-\nu_B)\sqrt{(1-\nu_A)^2+(1-\nu_B)^2}}{2-\nu_A-\nu_B}\right|\right].
\end{aligned} \tag{1}$$

Moreover, the (1) is rewritten as (2):

$$\begin{aligned}
d(A,B) = \frac{1}{2n}\sum_{i=1}^{n}\Bigg(&\left|\frac{(\mu_B(x_i)-\mu_A(x_i))\sqrt{\mu_A(x_i)^2+\mu_B(x_i)^2}}{\mu_B(x_i)+\mu_A(x_i)}\right| \\
&+ \left|\frac{((\nu_A(x_i)-\nu_B(x_i))\sqrt{(1-\nu_A(x_i))^2+(1-\nu_B(x_i))^2}}{2-\nu_A(x_i)-\nu_B(x_i)}\right|\Bigg).
\end{aligned} \tag{2}$$

Then, the similarity measure $s(A,B)$ is obtained as (3):

$$\begin{aligned}
s(A,B) = 1-\frac{1}{2n}\sum_{i=1}^{n}\Bigg(&\left|\frac{(\mu_B(x_i)-\mu_A(x_i))\sqrt{\mu_A(x_i)^2+\mu_B(x_i)^2}}{\mu_B(x_i)+\mu_A(x_i)}\right| \\
&+ \left|\frac{(\nu_A(x_i)-\nu_B(x_i))\sqrt{(1-\nu_A(x_i))^2+(1-\nu_B(x_i))^2}}{2-\nu_A(x_i)-\nu_B(x_i)}\right|\Bigg).
\end{aligned} \tag{3}$$

The proposed measure in (3) should satisfy the Definition 4, and the proof and conclusion are shown as follows.

Property 1: $0 \le s(A,B) \le 1$.

Proof: Because of $\min s(A,B) \le s(A,B) \le \max s(A,B)$, it can be proved by calculating the $\min s(A,B)$ and $\max s(A,B)$.

Based on (1), when $\overline{T_{\mu_B}N_1} = \overline{T_{\mu_A}N_1}$ and $\overline{T_{\nu_B}N_2} = \overline{T_{\nu_A}N_2}$, we can get $\min d_1 = 0$ and $\min d_2 = 0$. According to (3), we can get $\max s(A,B)$ as:

$$\max s(A,B) = 1 - \frac{1}{2}(\min d_1 + \min d_2) = 1 - \frac{1}{2}(0+0) = 1.$$

From Fig. 1, we can see that $0 \le \overline{T_\mu N_1} \le 1$ and $0 \le \overline{T_\nu N_2} \le 1$, then we can get $0 \le |\overline{T_{\mu_B}N_1} - \overline{T_{\mu_A}N_1}| \le 1$ and $0 \le |\overline{T_{\nu_B}N_2} - \overline{T_{\nu_A}N_2}| \le 1$, that is $\max d_i = 1$ (where $1 \le i \le 2$). Thus, $\min s(A,B)$ can be presented as:

$$\min s(A,B) = 1 - \frac{1}{2}(\max d_1 + \max d_2) = 1 - \frac{1}{2}(1+1) = 0.$$

Based on above analysis, we can get $0 \le s(A,B) \le 1$.

The proof of Property 1 is completed. □

Property 2: $s(A,B) = 1$ if and only if $A = B$.

Proof:

1) We should firstly proof a situation that: if $s(A,B) = 1$, then $A = B$.

Based on (1) and (3), the $d_1 = 0$ and $d_2 = 0$ must be satisfied simultaneously due to $d_1 \geq 0$ and $d_2 \geq 0$. We can get:

$$d_1 = \left| \frac{(\mu_B - \mu_A)\sqrt{{\mu_A}^2 + {\mu_B}^2}}{\mu_B + \mu_A} \right| = 0,$$

and

$$d_2 = \left| \frac{(\nu_A - \nu_B)\sqrt{(1-\nu_A)^2 + (1-\nu_B)^2}}{2 - \nu_A - \nu_B} \right| = 0.$$

Because of $\mu_B + \mu_A \geq 0$ and $2 - \nu_A - \nu_B \geq 0$ in the denominators of d_1 and d_2, the numerators must be 0 if $d = \frac{1}{2}(d_1 + d_2) = 0$ is satisfied. Let the numerators of d_1 and d_2 be a simultaneous system of equations as (4):

$$\begin{cases} (\mu_B - \mu_A)\sqrt{{\mu_A}^2 + {\mu_B}^2} = 0 \\ (\nu_A - \nu_B)\sqrt{(1-\nu_A)^2 + (1-\nu_B)^2} = 0 \end{cases}. \quad (4)$$

In (4), each equation can be divided into two cases, and the following two equation sets can be derived:

$$\begin{cases} ①\mu_B - \mu_A = 0 \quad \text{or} \quad ②{\mu_A}^2 + {\mu_B}^2 = 0 \\ ①\nu_A - \nu_B = 0 \quad \text{or} \quad ②(1-\nu_A)^2 + (1-\nu_B)^2 = 0 \end{cases},$$

$$\Rightarrow \begin{cases} ①\mu_B = \mu_A \quad \text{or} \quad ②\mu_A = 0 \text{ and } \mu_B = 0 \\ ①\nu_A = \nu_B \quad \text{or} \quad ②1 - \nu_A = 0 \text{ and } 1 - \nu_B = 0 \end{cases},$$

$$\Rightarrow \begin{cases} ①\mu_B = \mu_A \quad \text{or} \quad ②\mu_A = \mu_B = 0 \\ ①\nu_A = \nu_B \quad \text{or} \quad ②\nu_A = \nu_B = 1 \end{cases}.$$

From the above analysis, we can therefore get $\mu_A = \mu_B$ and $\nu_A = \nu_B$, which means $A = B$.

2) And then, we proof the second situation: if $A = B$, then $s(A, B) = 1$.
If $A = B$, $\mu_A = \mu_B$ and $\nu_A = \nu_B$. Then the u_A and v_A in (3) can be replaced with u_B and v_B, we can get:

$$\begin{aligned} s(A,B) &= 1 - \frac{1}{2}\left[\left| \frac{(\mu_A - \mu_A)\sqrt{{\mu_A}^2 + {\mu_A}^2}}{\mu_A + \mu_A} \right| \right. \\ &\quad \left. + \left| \frac{(\nu_A - \nu_A)\sqrt{(1-\nu_A)^2 + (1-\nu_A)^2}}{2 - \nu_A - \nu_A} \right| \right] \\ &= 1 - \frac{1}{2}\left[\left| \frac{0}{\mu_A + \mu_A} \right| + \left| \frac{0}{2 - \nu_A - \nu_A} \right| \right] \\ &= 1 \end{aligned}$$

From the above derivation, it can be obtained that $s(A, B) = 1$ if and only if $A = B$.
The proof of Property 2 is completed. □

Property 3: $s(A, B) = s(B, A)$.

Proof: The following equation transformation can be obtained due to the mathematical operation of absolute value:

$$\begin{aligned} s(A,B) &= 1 - \frac{1}{2}\left(\left| \frac{(\mu_B - \mu_A)\sqrt{{\mu_A}^2 + {\mu_B}^2}}{\mu_B + \mu_A} \right| \right. \\ &\quad \left. + \left| \frac{(\nu_A - \nu_B)\sqrt{(1-\nu_A)^2 + (1-\nu_B)^2}}{2 - \nu_A - \nu_B} \right| \right) \\ &= 1 - \frac{1}{2}\left(\left| -\frac{(\mu_B - \mu_A)\sqrt{{\mu_A}^2 + {\mu_B}^2}}{\mu_B + \mu_A} \right| \right. \\ &\quad \left. + \left| -\frac{(\nu_A - \nu_B)\sqrt{(1-\nu_A)^2 + (1-\nu_B)^2}}{2 - \nu_A - \nu_B} \right| \right) \\ &= 1 - \frac{1}{2}\left(\left| \frac{(\mu_A - \mu_B)\sqrt{{\mu_A}^2 + {\mu_B}^2}}{\mu_B + \mu_A} \right| \right. \\ &\quad \left. + \left| \frac{(\nu_B - \nu_A)\sqrt{(1-\nu_A)^2 + (1-\nu_B)^2}}{2 - \nu_A - \nu_B} \right| \right) \\ &= s(B,A). \end{aligned}$$

Then, the $s(A, B) = s(B, A)$ is obtained.
The proof of Property 3 is completed. □

Property 4: if $A \subseteq B \subseteq C$, then $s(A,C) \leq s(A,B)$ and $s(A,C) \leq s(B,C)$.

Proof: If $A \subseteq B \subseteq C$, then $0 \leq \mu_A \leq \mu_B \leq \mu_C \leq 1$ and $1 \geq \nu_A \geq \nu_B \geq \nu_C \geq 0$, that means $\mu_B - \mu_A \geq 0$ and $\nu_A - \nu_B \geq 0$. Therefore, we can get:

$$\frac{(\mu_B - \mu_A)\sqrt{{\mu_A}^2 + {\mu_B}^2}}{\mu_B + \mu_A} \geq 0,$$

and

$$\frac{(\nu_A - \nu_B)\sqrt{(1-\nu_A)^2 + (1-\nu_B)^2}}{2 - \nu_A - \nu_B} \geq 0.$$

Then, the (3) is simplified as follows:

$$\begin{aligned} & s(A,B) \\ &= 1 - \frac{1}{2}\left(\left| \frac{(\mu_B - \mu_A)\sqrt{{\mu_A}^2 + {\mu_B}^2}}{\mu_B + \mu_A} \right| \right. \\ &\quad \left. + \left| \frac{(\nu_A - \nu_B)\sqrt{(1-\nu_A)^2 + (1-\nu_B)^2}}{2 - \nu_A - \nu_B} \right| \right) \\ &= 1 - \frac{1}{2}\left(\frac{(\mu_B - \mu_A)\sqrt{{\mu_A}^2 + {\mu_B}^2}}{\mu_B + \mu_A} \right. \\ &\quad \left. + \frac{(\nu_A - \nu_B)\sqrt{(1-\nu_A)^2 + (1-\nu_B)^2}}{2 - \nu_A - \nu_B} \right) \end{aligned}$$

$$= 1 - \frac{1}{2}(s(A,B)_1 + s(A,B)_2).$$

Analogously, we can also obtain the simplifying form of $s(A,C)$ as follows:

$$\begin{aligned} & s(A,C) \\ &= 1 - \frac{1}{2}\left(\frac{(\mu_C - \mu_A)\sqrt{{\mu_A}^2 + {\mu_C}^2}}{\mu_C + \mu_A}\right. \\ &\quad \left. + \frac{(\nu_A - \nu_C)\sqrt{(1-\nu_A)^2 + (1-\nu_C)^2}}{2 - \nu_A - \nu_C}\right) \\ &= 1 - \frac{1}{2}\left(s(A,C)_1 + s(A,C)_2\right). \end{aligned}$$

Therefore, $s(A,B) - s(A,C)$ can be obtained as (5):

$$\begin{aligned} & s(A,B) - s(A,C) \\ &= 1 - \tfrac{1}{2}\left(s(A,B)_1 + s(A,B)_2\right) - 1 + \tfrac{1}{2}\left(s(A,C)_1 + s(A,C)_2\right) \\ &= \tfrac{1}{2}\left(s(A,C)_1 + s(A,C)_2\right) - \tfrac{1}{2}\left(s(A,B)_1 + s(A,B)_2\right) \\ &= \tfrac{1}{2}\left(s(A,C)_1 - s(A,B)_1\right) + \tfrac{1}{2}\left(s(A,C)_2 - s(A,B)_2\right). \end{aligned} \tag{5}$$

In (5), we first derive the equation $s(A,C)_1 - s(A,B)_1$, and then we can obtain the following results:

$$\begin{aligned} & s(A,C)_1 - s(A,B)_1 \\ &= \frac{(\mu_C - \mu_A)\sqrt{{\mu_A}^2 + {\mu_C}^2}}{\mu_C + \mu_A} - \frac{(\mu_B - \mu_A)\sqrt{{\mu_A}^2 + {\mu_B}^2}}{\mu_B + \mu_A} \\ &= \frac{(\mu_C - \mu_A)(\mu_B + \mu_A)\sqrt{{\mu_A}^2 + {\mu_C}^2} - (\mu_C + \mu_A)(\mu_B - \mu_A)\sqrt{{\mu_A}^2 + {\mu_B}^2}}{(\mu_C + \mu_A)(\mu_B + \mu_A)} \\ &= \frac{1}{(\mu_C + \mu_A)(\mu_B + \mu_A)}\left(\left(\mu_C\mu_B + \mu_C\mu_A - \mu_A\mu_B - {\mu_A}^2\right)\right. \\ &\quad \times \sqrt{{\mu_A}^2 + {\mu_C}^2} \\ &\quad \left. - \left(\mu_C\mu_B - \mu_C\mu_A + \mu_A\mu_B - {\mu_A}^2\right)\sqrt{{\mu_A}^2 + {\mu_B}^2}\right) \\ &= \frac{1}{(\mu_C + \mu_A)(\mu_B + \mu_A)}\left(\mu_C\mu_B(\sqrt{{\mu_A}^2 + {\mu_C}^2}\right. \\ &\quad - \sqrt{{\mu_A}^2 + {\mu_B}^2}) \\ &\quad - {\mu_A}^2(\sqrt{{\mu_A}^2 + {\mu_C}^2} - \sqrt{{\mu_A}^2 + {\mu_B}^2}) \\ &\quad + \mu_C\mu_A(\sqrt{{\mu_A}^2 + {\mu_C}^2} + \sqrt{{\mu_A}^2 + {\mu_B}^2}) \\ &\quad \left. - \mu_A\mu_B(\sqrt{{\mu_A}^2 + {\mu_C}^2} + \sqrt{{\mu_A}^2 + {\mu_B}^2})\right) \\ &= \frac{1}{(\mu_C + \mu_A)(\mu_B + \mu_A)}\left((\mu_C\mu_B - {\mu_A}^2)(\sqrt{{\mu_A}^2 + {\mu_C}^2}\right. \\ &\quad - \sqrt{{\mu_A}^2 + {\mu_B}^2}) \\ &\quad \left. + (\mu_C\mu_A - \mu_A\mu_B)(\sqrt{{\mu_A}^2 + {\mu_C}^2} + \sqrt{{\mu_A}^2 + {\mu_B}^2})\right). \end{aligned}$$

From the above equation, we can get:

$$\begin{cases} \mu_C\mu_B - {\mu_A}^2 \geq 0 \text{ and } \sqrt{{\mu_A}^2 + {\mu_C}^2} - \sqrt{{\mu_A}^2 + {\mu_B}^2} \geq 0 \\ \mu_C\mu_A - \mu_A\mu_B \geq 0 \text{ and } \sqrt{{\mu_A}^2 + {\mu_C}^2} + \sqrt{{\mu_A}^2 + {\mu_B}^2} \geq 0, \\ (\mu_C + \mu_A)(\mu_B + \mu_A) \geq 0 \end{cases}$$

and then, we can get:

$$\begin{cases} (\mu_C\mu_B - {\mu_A}^2)(\sqrt{{\mu_A}^2 + {\mu_C}^2} - \sqrt{{\mu_A}^2 + {\mu_B}^2}) \geq 0 \\ (\mu_C\mu_A - \mu_A\mu_B)(\sqrt{{\mu_A}^2 + {\mu_C}^2} + \sqrt{{\mu_A}^2 + {\mu_B}^2}) \geq 0. \\ (\mu_C + \mu_A)(\mu_B + \mu_A) \geq 0 \end{cases}$$

Therefore, $s(A,C)_1 - s(A,B)_1 \geq 0$ is obtained.

For $s(A,C)_2 - s(A,B)_2$, because of $(\nu_A - \nu_C)(2 - \nu_A - \nu_B) \geq 0$ and $1 - \nu_C \geq 1 - \nu_B$, we can get the following derivations:

$$\begin{aligned} & s(A,C)_2 - s(A,B)_2 \\ &= \frac{1}{(2 - \nu_A - \nu_C)(2 - \nu_A - \nu_B)}\left((\nu_A - \nu_C)(2 - \nu_A - \nu_B)\right. \\ &\quad \times \sqrt{(1-\nu_A)^2 + (1-\nu_C)^2} \\ &\quad \left. - (\nu_A - \nu_B)(2 - \nu_A - \nu_C)\sqrt{(1-\nu_A)^2 + (1-\nu_B)^2}\right) \\ &\geq \frac{1}{(2 - \nu_A - \nu_C)(2 - \nu_A - \nu_B)}\left((\nu_A - \nu_C)(2 - \nu_A - \nu_B)\right. \\ &\quad \times \sqrt{(1-\nu_A)^2 + (1-\nu_B)^2} \\ &\quad \left. - (\nu_A - \nu_B)(2 - \nu_A - \nu_C)\sqrt{(1-\nu_A)^2 + (1-\nu_B)^2}\right) \\ &= \frac{1}{(2 - \nu_A - \nu_C)(2 - \nu_A - \nu_B)} \\ &\quad \times \left((2\nu_A - {\nu_A}^2 - \nu_A\nu_B - 2\nu_C + \nu_A\nu_C + \nu_B\nu_C)\right. \\ &\quad \times \sqrt{(1-\nu_A)^2 + (1-\nu_B)^2} \\ &\quad - (2\nu_A - {\nu_A}^2 - \nu_A\nu_C - 2\nu_B + \nu_A\nu_B + \nu_B\nu_C) \\ &\quad \left. \times \sqrt{(1-\nu_A)^2 + (1-\nu_B)^2}\right) \\ &= \frac{1}{(2 - \nu_A - \nu_C)(2 - \nu_A - \nu_B)} \\ &\quad \times \left((-2\nu_A\nu_B - 2\nu_C + 2\nu_A\nu_C + 2\nu_B)\right. \\ &\quad \left. \times \sqrt{(1-\nu_A)^2 + (1-\nu_B)^2}\right) \\ &= \frac{1}{(2 - \nu_A - \nu_C)(2 - \nu_A - \nu_B)} \\ &\quad \times \left(2(\nu_B - \nu_C)(1 - \nu_A)\sqrt{(1-\nu_A)^2 + (1-\nu_B)^2}\right). \end{aligned}$$

Because of $\nu_B - \nu_C \geq 0$, $1-\nu_A \geq 0$, and $(1-\nu_A)^2 + (1-\nu_B)^2 \geq 0$, we can get:

$$\begin{cases} (\nu_B - \nu_C)(1-\nu_A)\sqrt{(1-\nu_A)^2 + (1-\nu_B)^2} \geq 0 \\ (2-\nu_A-\nu_C)(2-\nu_A-\nu_B) \geq 0 \end{cases}.$$

Thus, $s(A,C)_2 - s(A,B)_2 \geq 0$ is obtained, and then we can get the final result as follows:

$$\begin{aligned} & s(A,B) - s(A,C) \\ &= \tfrac{1}{2}\left[s(A,C)_1 - s(A,B)_1\right] + \tfrac{1}{2}\left[s(A,C)_2 - s(A,B)_2\right] \\ &\geq 0. \end{aligned}$$

Therefore, $s(B,C) \geq s(A,C)$ is also obtained according to the same derivation.

The proof of Property 4 is completed. □

Property 5: If A is a crisp set, then $s(A, A^C) = 0$.

Proof: If A is a crisp set, then $\mu_A = 1, \mu_{A^C} = 0$ and $\nu_A = 0$, $\nu_{A^C} = 1$. Therefore, we can get:

$$\begin{aligned} & s(A, A^C) \\ &= 1 - \frac{1}{2}\left[\left|\frac{(\mu_{A^C} - \mu_A)\sqrt{{\mu_A}^2 + {\mu_{A^C}}^2}}{\mu_{A^C} + \mu_A}\right| \right. \\ &\quad \left. + \left|\frac{(\nu_A - \nu_{A^C})\sqrt{(1-\nu_A)^2 + (1-\nu_{A^C})^2}}{2 - \nu_A - \nu_{A^C}}\right|\right] \\ &= 1 - \frac{1}{2}\left[\left|\frac{(0-1)\sqrt{1^2+0^2}}{0+1}\right| + \left|\frac{(0-1)\sqrt{1^2+0^2}}{2-1-0}\right|\right] \\ &= 1 - \frac{1}{2}\left[|-1| + |-1|\right] \\ &= 0. \end{aligned}$$

The proof of Property 5 is completed. □

Corollary 1: Given two IFSs $A = \{\langle x_i, \mu_A(x_i), \nu_A(x_i)| x_i \in X\}$ and $B = \{\langle x_i, \mu_B(x_i), \nu_B(x_i)\rangle | x_i \in X\}$ in the domain of $X = \{x_1, x_2, \ldots, x_n\}$, and the similarity between IFSs A and B is represented as follows:

$$s_{LJ}(A,B) = \sum_{i=1}^{n} w_i s_i,$$

where w_i is the weight of s_i with the constraint $\sum_{i=1}^{n} w_i = 1$.

B. Our Proposed Medical Image Fusion Method via the Similarity Measure of IFSs

A lightweight medical image fusion method based on the proposed similarity measure of IFSs is introduced in this subsection. Because of the strong power of IFS theory for analyzing the imprecise and vague features in an image, this work introduces the new proposed similarity measure of IFSs into medical image fusion. In medical image fusion, the pixel fusion weight of each source image is the key point, and the weights are usually relate to the features of the pixel and its neighboring pixels [16]. Therefore, the source medical images are first decomposed by LPD to obtain a set of sub-band coefficients (or sub-band images), and the sub-band coefficients are considered as the components of the source image pixels. Then, our fusion rule based on the proposed similarity measure is employed to confirm which sub-band coefficient should be kept. At last, the fused medical image is recovered according to the fused sub-band coefficients by inverse LPD. Fig. 2 shows the proposed fusion method.

1) Laplacian Pyramid Decomposition of Medical Image: The LPD [16] is a classical analysis method for presenting the features of a source image. A LPD is performed on the basis of Gaussian pyramid decomposition (GPD), and the GPD is therefore conducted firstly. Given a source image G_0, Gaussian low-pass filter and down-sampling operations are conducted on G_0 to get next layer. Thus, the next layer l-th is got by (6):

$$G_l(i,j) = \sum_{m=-2}^{2}\sum_{n=-2}^{2} \omega(m,n) G_{l-1}(2i+m, 2j+n), \quad (6)$$

where $1 \leq l \leq N$, $0 \leq i < R_l$, $0 \leq j < C_l$ (N is the layer number of GPD, and R_i and C_i respectively present the row and column of the l-th layer in GPD); $G_l(i,j)$ is the GPD pixel of the position (i,j) at the l-th layer; $\omega(m,n)$ denotes a given Gaussian matrix with the size of 5×5, as (7):

$$\omega = \frac{1}{256}\begin{bmatrix} 1 & 4 & 6 & 4 & 1 \\ 4 & 16 & 24 & 16 & 4 \\ 6 & 24 & 36 & 24 & 6 \\ 4 & 16 & 24 & 16 & 4 \\ 1 & 4 & 6 & 4 & 1 \end{bmatrix}. \quad (7)$$

Because of the down sampling operation in GPD, the size of G_l is a quarter to that of the G_{l-1}. If the interpolation is performed on G_l to get G_l^*, the size of G_l^* will be the same as that of G_{l-1}, as (8):

$$G_l^*(i,j) = 4\sum_{m=-2}^{2}\sum_{n=-2}^{2} \omega(m,n) G_l\left(\frac{i+m}{2}, \frac{j+n}{2}\right), \quad (8)$$

where, $0 < l \leq N, 0 \leq i < R_l, 0 \leq j < C_l$, and

$$\begin{aligned} & G_l\left(\frac{i+m}{2}, \frac{j+n}{2}\right) \\ &= \begin{cases} G_l\left(\frac{i+m}{2}, \frac{j+n}{2}\right), & \frac{i+m}{2} \text{ and } \frac{j+n}{2} \text{ are integer} \\ 0, & \text{other} \end{cases}. \end{aligned} \quad (9)$$

Thus, the LPD can be presented as (10):

$$\begin{cases} LP_l = G_l - G_{l+1}^*, & 0 \leq l < N \\ LP_N = G_N, & l = N \end{cases}, \quad (10)$$

where N denotes the total number of LPD layers; G_l presents the l-th layer of GPD, and G_{l+1}^* is the l-th dilated layer; LP_l is the l-th layer of LPD.

According to (10), each layer of LPD is enlarged by the interpolation operation on GPD; thus, the size of the current layer is the same as its next layer. Therefore, the final medical image can be obtained by adding all these layers one after the other, and the inverse of LPD can be presented as (11):

$$\begin{cases} G_N = LP_N, & l = N \\ G_l = LP_l + G_{l+1}^*, & 0 \leq l < N \end{cases}. \quad (11)$$

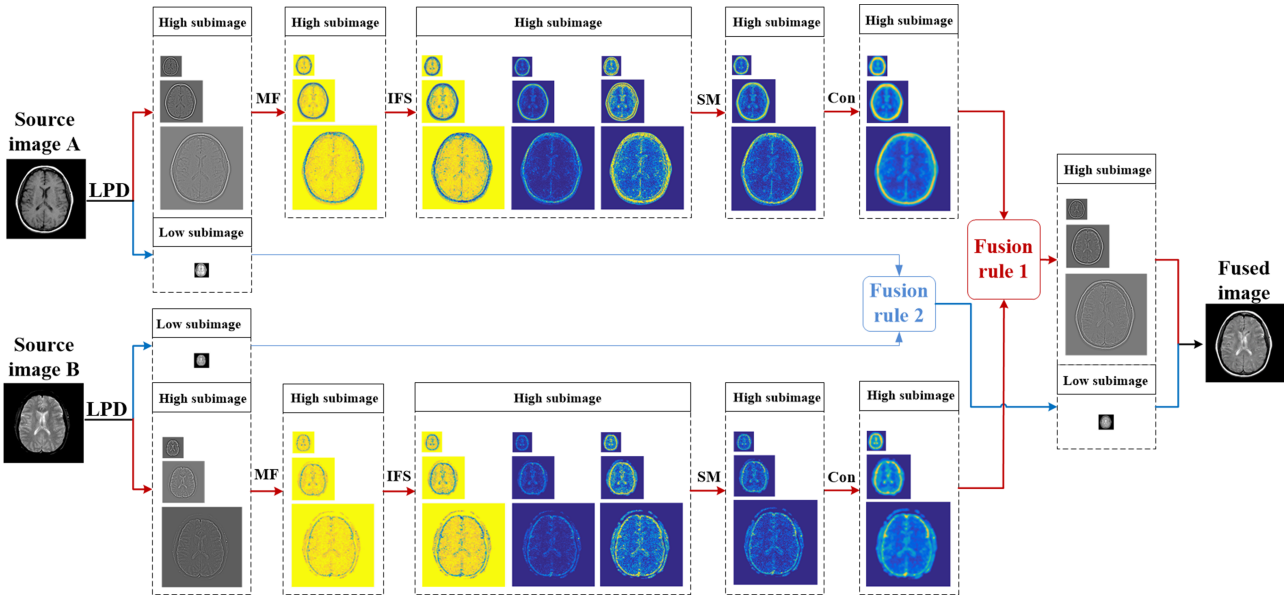

Fig. 2. The proposed medical image fusion scheme.

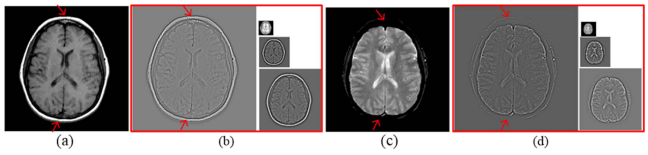

Fig. 3. Example of LPD. (a) Source medical image A; (b) The corresponding coefficients of sub-images of source medical image A; (c) Source medical image B; (d) The corresponding coefficients of sub-images of source medical image B.

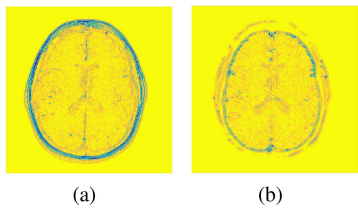

Fig. 4. The example of membership matrix. (a) The membership matrix of sub-images A; (b) The membership matrix of sub-images B.

Two examples of three-layer LPD are given in Fig. 3, and Fig. 3(b) and (d) show that LPD can describe the significant features of the medical images A and B. Specifically, the edges and detailed information of the medical images can be clearly presented in these sub-images. In this method, a three-layer of LPD is employed based on our numerous attempts, which has acceptable computation with competitive performance.

2) Feature Extraction of Sub-Band Coefficients Based on IFSs: The similarity of FS has outstanding capacity to measure and address the imprecise information in various fields, such as image processing [17]. This work proposes a novel lightweight fusion method based on fuzzy similarity measure that is utilized to represent medical image features.

First, the fuzzification of sub-band coefficients are performed by a given membership function that is triangular MF [28], which is expressed as (12):

$$\mu_{FS}(im(i,j)) = \begin{cases} 0, & im(i,j) \le a | c \le im(i,j) \\ (im(i,j)-a)/(b-a), & a < im(i,j) \& im(i,j) < b \\ (c-im(i,j))/(c-b), & b < im(i,j) \& im(i,j) < c \end{cases} \tag{12}$$

where $im(i,j)$ denotes the pixel value, and $\mu_{FS}(im(i,j))$ is corresponding to MF; $|$ and & are respectively logical OR and AND operation. Moreover, a, b, and c are respectively the minimum, mean, and maximum value in $im(i,j)$.

From (12), we can know that the parameters of membership function need to be calculated firstly. To keep the consistency of the fuzzification of sub-band coefficients obtained by different source images, the corresponding sub-band coefficients are concatenated, and then the parameters a, b, and c can be obtained according to the concatenated coefficient matrix, as shown in (13)–(15):

$$a = \min\left(\text{concatenated}\left\langle im^A, im^B \right\rangle\right), \tag{13}$$

$$b = \text{mean}\left(\text{concatenated}\left\langle im^A, im^B \right\rangle\right), \tag{14}$$

$$c = \max\left(\text{concatenated}\left\langle im^A, im^B \right\rangle\right), \tag{15}$$

where im^A and im^B are the sub-band coefficients from medical images A and B, respectively.

Fig. 4 shows the membership matrices of sub-images A and B. We can get that the unique features of each sub-image are effectively extracted. Besides, the membership matrices of FSs of different sub-images can be further transformed into the membership matrices of IFSs, which are expressed as (16)–(18):

$$\mu_{IFS}(im(i,j)) = [\mu_{FS}(im(i,j))]^{\alpha}, \tag{16}$$

$$\nu_{IFS}(im(i,j)) = 1 - [\mu_{FS}(im(i,j))]^{1/\alpha}, \tag{17}$$

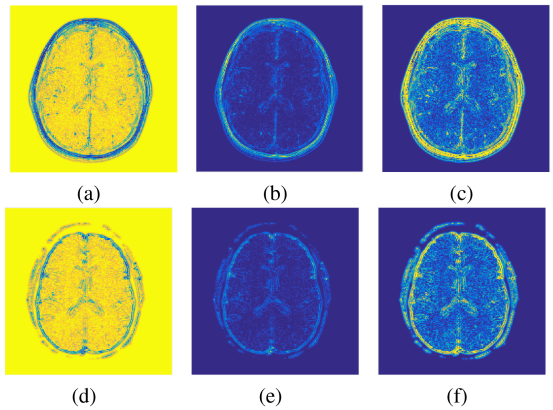

Fig. 5. The membership matrices of IFSs of sub-images A and B. (a) The membership matrix μ_A of sub-image A; (b) The non-membership matrix ν_A of sub-image A; (c) The hesitancy matrix π_A of sub-image A; (d) The membership matrix μ_B of sub-image B; (e) The non-membership matrix ν_B of sub-image B; (f) The hesitancy matrix π_B of sub-image B.

$$\pi_{IFS}(im(i,j)) = [\mu_{FS}(im(i,j))]^{1/\alpha} - [\mu_{FS}(im(i,j))]^{\alpha}, \tag{18}$$

where $\alpha = 2$.

Moreover, the membership matrices of IFSs of the sub-images A and B are respectively shown in Fig. 5, which shows that the key features are better enhanced compared with the membership matrices of FSs in Fig. 4.

To confirm which sub-band coefficients from the two different source images should be kept, a targeted scheme is designed based on our novel similarity measure of IFSs. First, we transform the image pixel values into IFSs according to (12)–(18). The idea is shown as: if we have a crisp intuitionistic fuzzy set C (which means $\mu_C = 1$, $v_C = 0$ and $\pi_C = 0$), we can respectively measure the similarity between two unknown elements (coefficients) with the given crisp intuitionistic fuzzy set (IFS C). Thus, we can determine the two unknown elements (IFSs A and B). The similarity between the IFSs A and C is shown as (19), and the similarity between the IFSs B and C is shown as (20):

$$\begin{aligned} &s_{LJ\_AC}(i,j) \\ &= 1 - \frac{1}{2n}\sum_{i=1}^{n}\left(\left| \frac{(\mu_C - \mu_{A_{IFS}}(im(i,j)))\sqrt{\mu_{A_{IFS}}(im(i,j))^2 + \mu_C{}^2}}{\mu_C + \mu_{A_{IFS}}(im(i,j))} \right| \right. \\ &\quad \left. + \left| \frac{(\nu_{A_{IFS}}(im(i,j)) - \nu_C)\sqrt{\left(1-\nu_{A_{IFS}}(im(i,j))\right)^2 + (1-\nu_C)^2}}{2 - \nu_{A_{IFS}}(im(i,j)) - \nu_C} \right| \right), \end{aligned} \tag{19}$$

$$\begin{aligned} &s_{LJ\_BC}(i,j) \\ &= 1 - \frac{1}{2n}\sum_{i=1}^{n}\left(\left| \frac{(\mu_C - \mu_{B_{IFS}}(im(i,j)))\sqrt{\mu_{B_{IFS}}(im(i,j))^2 + \mu_C{}^2}}{\mu_C + \mu_{B_{IFS}}(im(i,j))} \right| \right. \\ &\quad \left. + \left| \frac{(\nu_{B_{IFS}}(im(i,j)) - \nu_C)\sqrt{\left(1-\nu_{B_{IFS}}(im(i,j))\right)^2 + (1-\nu_C)^2}}{2 - \nu_{B_{IFS}}(im(i,j)) - \nu_C} \right| \right), \end{aligned} \tag{20}$$

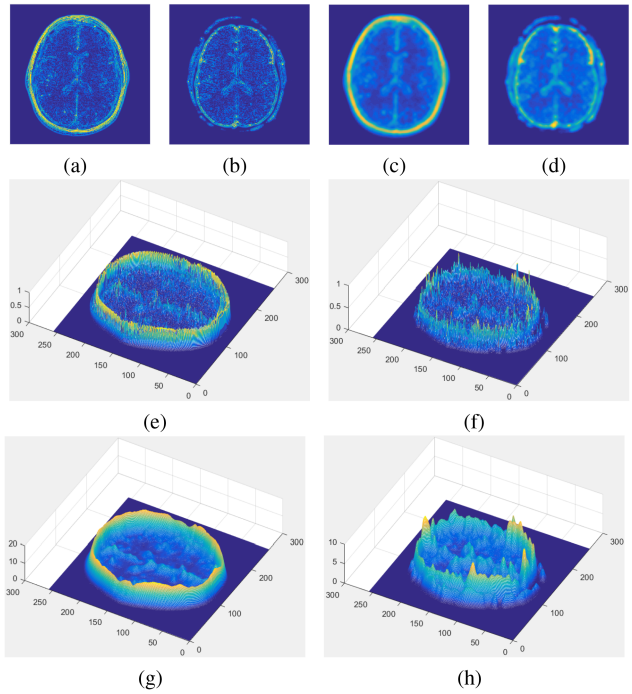

Fig. 6. The similarity matrices of sub-images A and B. (a) (e) The similarity matrix of sub-image A; (b) (f) The similarity matrix of sub-image B; (c) (g) The similarity matrix after convolution operation of sub-image A; (d) (h) The similarity matrix after convolution operation of sub-image A.

where s_{LJ_AC} is the similarity between IFSs A and C, s_{LJ_BC} is the similarity between IFSs B and C.

Thus, the similarity of IFS is used to measure the features of an image. For nonlinear human vision, the importance of a single pixel is closely related to its adjacent pixels. To combine the information of pixel and its neighboring pixels, a convolution operation is respectively used for the similarity matrix of medical images A as (21) and B as (22):

$$CS_{AC}(i,j) = \sum_{m}^{2}\sum_{n}^{2}\omega(m,n)s_{LJ\_AC}(i,j), \tag{21}$$

$$CS_{BC}(i,j) = \sum_{m}^{2}\sum_{n}^{2}\omega(m,n)s_{LJ\_BC}(i,j), \tag{22}$$

where ω is a given convolution kernel; CS is the convolutional similarity matrix.

Fig. 6 shows that the similarity matrices and their corresponding convolution matrices of sub-images A and B. From Fig. 6(a) and (b), we can find that the similarity matrices are effective to describe and extract the feature information of these medical images. But the features can obviously present the discrete distribution of similarity matrices of sub-images A and B, which can be found clearly from the 3D plots of the similarity matrices of these sub-band images, as Fig. 6(e) and (f). However, the fused image generated by the similarity matrices of sub-images A and B may be not satisfactory because the regional information is ignored. The similarity matrices after convolution operation are displayed in Fig. 6(c) and (d), which indicate that the relationship among the surrounding pixels are established compared with the

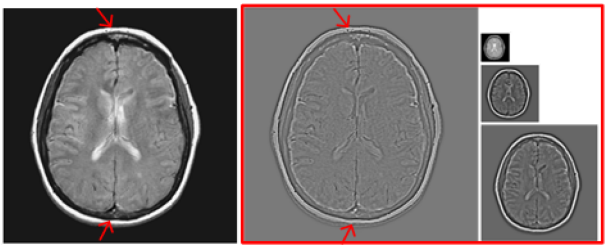

Fig. 7. Fused image and the corresponding fused sub-band images.

discrete similarity matrices in Fig. 6(a) and (b), and the regional features of the images are therefore effectively presented. This experiment reveals that the proposed similarity between IFSs is beneficial to present medical image features.

3) The Fusion Rules of Sub-Images: The high frequency sub-band images (or sub-band coefficients) present the details of medical images and are important for human visual system. In general, the details in high frequency sub-image are difficult to fuse them directly because they are fine features in small scale. The quantification of the importance of these features is the key issue to fuse them. In this work, we employ IFSs-based measure to quantize the features of high frequency sub-images, so that a sample rule is then used for fusing them, and the operation is defined as (23):

$$FHC = \begin{cases} HC_A, & (HCS_{AC} > HCS_{AB}) \\ HC_B, & (HCS_{AC} < HCS_{AB}) \\ (HC_A + HC_B)/2, & (HCS_{AC} = HCS_{AB}) \end{cases}, \tag{23}$$

where FHC is the fused high frequency sub-band coefficients; HC_A and HC_B are the high frequency sub-band coefficients from medical images A and B, respectively; HCS is the high frequency convolutional similarity matrix.

The low frequency sub-image presents the approximate features of the medical images, and the amplitude of the coefficient can provide enough information to fuse them. Therefore, we employ a simple fusion rule to deal with them, the operation is defined as (24):

$$FLC = \begin{cases} LC_A, & abs\,(LC_A) \geq abs(LC_B) \\ LC_B, & abs\,(LC_A) < abs(LC_B) \end{cases}, \tag{24}$$

where FLC represents the fused low frequency sub-band coefficients; LC_A and LC_B are respectively the low frequency sub-band coefficients from medical images A and B.

The fused low and high frequency sub-images are presented in Fig. 7. Compared with Fig. 3, the details of sub-images of different source medical images are fused effectively, such as the features of skeleton and the textures of brain in Fig. 7.

IV. Experiments and Analysis

The effectiveness of our method is verified by numerical experiments and medical image fusion experiments.

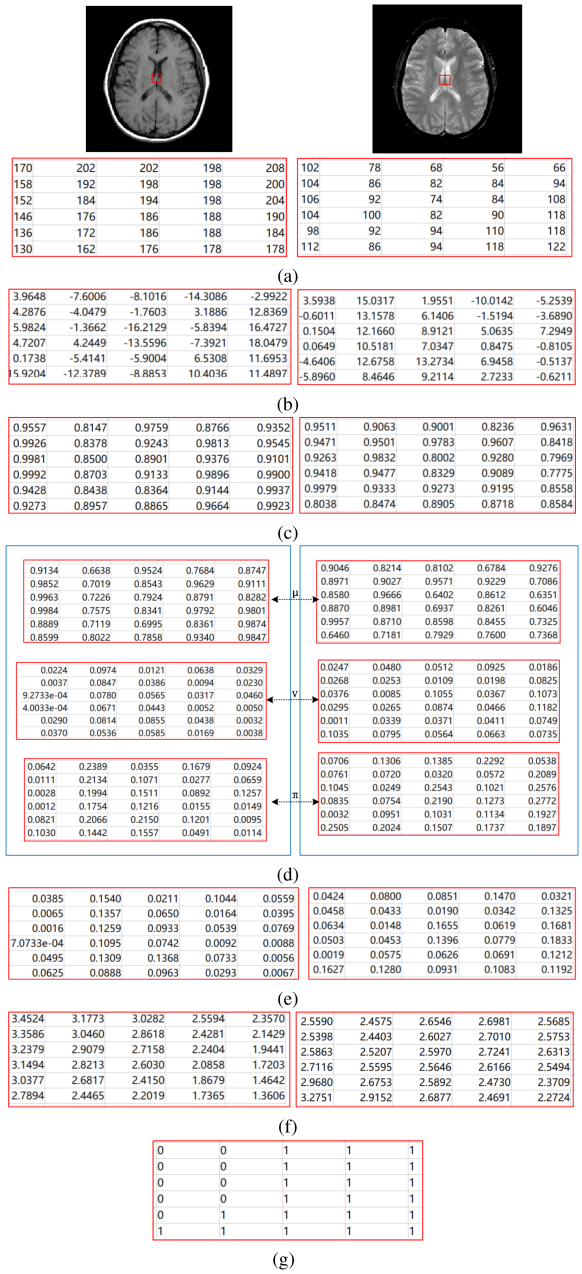

Fig. 8. Examples of medical image fusion. (a) Source images and the pixels; (b) The coefficients in the first layer in LPD; (c) The membership degrees of the first layer coefficients; (d) The membership, nonmembership, and hesitancy of IFSs from the first layer coefficients; (e) Similarity between two different medical images and the crisp IFS C; (f) Convolutional similarity matrix of the first similarity matrix; (g) The fusion decisions.

A. Numerical Experiments of Similarity Measures

The numerical experiments for fuzzy similarity measure usually have two forms: fuzzy set experiment and pattern recognition experiment. In this paper, eighteen classic similarity or distance measures are selected to contrast with the proposed measure: $S_C(A,B)$[29], $S_{HK}(A,B)$[30], $S_{DC}(A,B)$[25], $S^E_{LS}(A,B)$[31], $S^S_{LS}(A,B)$[31], $S^H_{LS}(A,B)$ [31], $S_M(A,B)$[32], $S^l_{HY1}(A,B)$ [12], $S^e_{HY1}(A,B)$ [12], $S^c_{HY1}(A,B)$ [12], $d_{WX}(A,B)$[33], $S_Y(A,B)$ [13], $S_F(A,B)$

TABLE I
THE FUZZY SET EXPERIMENTAL DATA FOR DIFFERENT MEASURES

Case	the first six pairs of IFSs		the second six pairs of IFSs	
	A_1	B_1	A_2	B_2
case1	<0.3,0.3>	<0.4,0.4>	<0.5,0.5>	<0.0,0.0>
case2	<0.3,0.4>	<0.4,0.4>	<0.6,0.4>	<0.0,0.0>
case3	<1.0,0.0>	<0.0,0.0>	<0.0,0.87>	<0.28,0.55>
case4	<0.5,0.5>	<0.0,0.0>	<0.6,0.27>	<0.28,0.55>
case5	<0.4,0.2>	<0.5,0.3>	<0.125,0.075>	<0.175,0.025>
case6	<0.4,0.2>	<0.5,0.2>	<0.5,0.45>	<0.55,0.40>

TABLE II
THE FIRST EXPERIMENTAL RESULTS OF DIFFERENT MEASURES

measures	case1	case2	case3	case4	case5	case6
S_C	**1**	0.9000	0.5000	**1**	**1**	0.9500
S_{HK}	**0.9000**	**0.9000**	**0.5000**	**0.5000**	**0.9000**	0.9500
S_{DC}	**1**	0.9000	0.5000	**1**	**1**	0.9500
S_{LS}^{E}	**0.9000**	**0.9000**	**0.5000**	**0.5000**	**0.9000**	0.9500
S_{LS}^{S}	**0.9500**	0.9000	0.5000	0.7500	**0.9500**	**0.9500**
S_{LS}^{H}	**0.9333**	**0.9333**	0.5000	0.6667	**0.9333**	0.9500
S_M	**0.9000**	**0.9000**	**0.5000**	**0.5000**	**0.9000**	0.9500
S_{HY1}^{l}	**0.9000**	**0.9000**	**0.5000**	**0.5000**	**0.9000**	0.9500
S_{HY1}^{e}	**0.7904**	**0.7904**	**0.2689**	**0.2689**	**0.7904**	0.8899
S_{HY1}^{c}	**0.7500**	**0.7500**	**0.2500**	**0.2500**	**0.7500**	0.8636
d_{WX}	**0.9000**	**0.9000**	0.2500	0.5000	**0.9000**	0.9250
S_Y	1.0000	0.9600	NaN	NaN	0.9971	0.9965
D_{BA}	**0.9667**	0.9000	0.5000	0.8333	**0.9667**	0.9500
S_F	0.8268	-1.0000	0	0.1340	0.8292	0.9047
S_{CCL}	**0.9667**	0.9000	0.5000	0.8333	**0.9667**	0.9450
S_{GK}	**0.9600**	0.9333	0.3333	0.6667	**0.9600**	0.9467
D_{Hm}	0.9333	0.9000	0.3333	0.6667	0.9000	0.9333
S_{JJ}	0.9490	0.8977	0.5000	0.7500	0.9592	0.9450
D_{AS}^{P}	0.9600	0.9091	**0**	**0**	0.9362	0.9730
S_{LJ}	0.9423	0.9400	0.5000	0.5637	0.9391	0.9644

($p = 1$ in S_{DC}, S_{LS}^{E}, S_{LS}^{S}, S_{LS}^{H}, S_M and D_{BA}; $t = 2$ in D_{BA})

TABLE III
THE SECOND EXPERIMENTAL RESULTS OF DIFFERENT MEASURES

measures	case1	case2	case3	case4	case5	case6
S_C	1	0.9000	**0.7000**	**0.7000**	**0.9500**	**0.9500**
S_{HK}	**0.5000**	**0.5000**	**0.7000**	**0.7000**	**0.9500**	**0.9500**
S_{DC}	1	0.9000	**0.7000**	**0.7000**	**0.9500**	**0.9500**
S_{LS}^{E}	**0.5000**	**0.5000**	**0.7000**	**0.7000**	**0.9500**	**0.9500**
S_{LS}^{S}	**0.7500**	**0.7500**	**0.7000**	**0.7000**	**0.9500**	**0.9500**
S_{LS}^{H}	0.6667	0.6333	**0.7933**	**0.7933**	**0.9667**	**0.9667**
S_M	**0.5000**	**0.5000**	**0.7000**	**0.7000**	**0.9500**	**0.9500**
S_{HY1}^{l}	**0.5000**	**0.5000**	**0.7000**	**0.7000**	**0.9500**	**0.9500**
S_{HY1}^{e}	**0.2689**	**0.2689**	**0.4782**	**0.4782**	**0.8899**	**0.8899**
S_{HY1}^{c}	**0.2500**	**0.2500**	**0.4375**	**0.4375**	**0.8636**	**0.8636**
d_{WX}	0.5000	0.4500	**0.6900**	**0.6900**	**0.9500**	**0.9500**
S_Y	NaN	NaN	0.8912	0.7794	0.9216	0.9946
D_{BA}	**0.8333**	**0.8333**	**0.7000**	**0.7000**	**0.9500**	**0.9500**
S_F	0.1340	0.1282	0.8614	-0.9601	0.9863	0.9970
S_{CCL}	**0.8333**	**0.8333**	0.7047	0.6953	**0.9500**	**0.9500**
S_{GK}	0.6667	0.6533	0.6840	0.7920	**0.9633**	**0.9633**
D_{Hm}	0.6667	0.6000	**0.6933**	**0.6933**	**0.9500**	**0.9500**
S_{JJ}	0.7500	0.8000	**0.6983**	**0.6983**	0.9405	0.9500
D_{AS}^{P}	**0**	**0**	0.8335	0.5450	0.6000	0.9843
S_{LJ}	0.5637	0.5542	0.8154	0.8270	0.9648	0.9719

($p = 1$ in S_{DC}, S_{LS}^{E}, S_{LS}^{S}, S_{LS}^{H}, S_M and D_{BA}; $t = 2$ in D_{BA})

TABLE IV
THE PATTERN RECOGNITION EXPERIMENTAL DATA FOR DIFFERENT MEASURES

Elements	Case1			
	A_1	A_2	A_3	B
x1	<0.5,0.4>	<0.6,0.3>	<0.6,0.3>	<0.0,0.0>
x2	<0.8,0.0>	<0.9,0.1>	<0.9,0.1>	<0.0,0.0>
x3	<0.3,0.7>	<0.6,0.4>	<0.5,0.5>	<0.0,0.1>
Elements	Case2			
	A_1	A_2	A_3	B
x1	<0.34,0.34>	<0.35,0.33>	<0.33,0.35>	<0.37,0.31>
x2	<0.19,0.48>	<0.20,0.47>	<0.21,0.46>	<0.23,0.44>
x3	<0.02,0.12>	<0.0,0.14>	<0.01,0.13>	<0.04,0.1>

[14], $S_{CCL}(A,B)$ [11], $D_{BA}(A,B)$ [34], $D_{Hm}(A,B)$ [35], $S_{GK}(A,B)$[36], $S_{JJ}(A,B)$ [37], and $D_{AS}^{P}(A,B)$[38].

1) Similarity Experiments: The similarity experiments on different measures are respectively performed to present the similarity between two IFSs, which is used to verify the effectiveness of our measure $S_{LJ}(A,B)$. Generally, a good similarity measure should differentiate the degree of similarity between different IFSs accurately, and the popular experiment contains two cases which are frequently used in this field to test the effectiveness of fuzzy measures [11], [13], [14], [37], and each one has six different pairs of IFSs A and B.

The first and second six pairs of experimental IFSs A and B are presented in Table I. The results of the first six pairs of IFSs A and B are shown in Tables II, and the results of the second six pairs of IFSs A and B are shown in Tables III, in these tables the counter-intuitive results are marked by bold characters. In Tables II and III, most previous measures produce unreasonable results because the same values are got by some (or all) cases, which cannot differentiate the similar degree. For example, Chen's similarity measure S_C has the equal degree of similarity in Cases 1, 4 and 5 for Table II; besides, the same similarity can be also found in Cases 3 and 4, and Cases 5 and 6 for Table III. Moreover, this drawback also exists in other measures. In addition, S_Y cannot make decisions because the divisor is 0. Tables II and III show that the proposed measure S_{LJ} can generate reasonable decisions, which means it can get better performance than the contrast measures.

2) Pattern Recognition Experiment: The similarity measure of IFSs can be employed for pattern recognition by calculating the similarity degree of samples. Therefore, some commonly used pattern recognition cases are utilized to verify the performance of our measure. And a good similarity measure should output reasonable decisions to recognize the relationship among multi-patterns, the experiments are shown as follows.

Consider two cases from Refs. [13], [14] with three given patterns A_1, A_2 and A_3 in universe $X = \{x_1, x_2, x_3\}$, and a given sample B that needs to be identified. The experimental data of three patterns and sample B are given as Table IV.

In this experiment, the similarity measure is utilized to classify sample B into one of the three given patterns. According to the references [11], [14], the sample B should be classified into pattern A1 in both two cases. We set the weight w_i to 1/3 in all measures, and the results of pattern recognition are shown in Table V. According to similarity theory, the sample B should be classified into one of the given pattern that has the maximal similarity value. From Table V, we can see that most of the previous measures do not make a right decision for recognizing the pattern of IFS B, and there are two reasons: the first one is that some measures have the same maximal similarity value in different patterns, for example, the S_C in Cases 1 and 2, and S_{HK} in Case 2; and the second reason is that some measures do not get the measurement result, for example, S_Y has the problem that the divisor is 0. In addition, some measures have the different

TABLE V
THE PATTERN RECOGNITION RESULTS OF DIFFERENT MEASURES

measures	case 1				case 2			
	$S(A_1, B)$	$S(A_2, B)$	$S(A_3, B)$	Classification result	$S(A_1, B)$	$S(A_2, B)$	$S(A_3, B)$	Classification result
S_C	0.8000	0.7667	0.8000	Undetermined	0.9700	0.9700	0.9700	Undetermined
S_{HK}	0.5667	0.5333	0.5333	A1	0.9700	0.9700	0.9700	Undetermined
S_{DC}	0.8000	0.7667	0.8000	Undetermined	0.9700	0.9700	0.9700	Undetermined
S_{LS}^{E}	0.5667	0.5333	0.5333	A1	0.9700	0.9700	0.9700	Undetermined
S_{LS}^{S}	0.7167	0.7167	0.7167	Undetermined	0.9700	0.9700	0.9700	Undetermined
S_{LS}^{H}	0.6444	0.6111	0.6222	A1	0.9800	0.9800	0.9800	Undetermined
S_M	0.5667	0.5333	0.5333	A1	0.9700	0.9700	0.9700	Undetermined
S_{HY1}^{l}	0.5667	0.5333	0.5333	A1	0.9700	0.9700	0.9700	Undetermined
S_{HY1}^{e}	0.3302	0.2988	0.2988	A1	0.9328	0.9328	0.9328	Undetermined
S_{HY1}^{α}	0.3041	0.2763	0.2763	A1	0.9154	0.9154	0.9154	Undetermined
d_{WX}	0.4667	0.4167	0.4333	A1	0.9700	0.9700	0.9700	Undetermined
S_Y	N/A	N/A	N/A	Undetermined	0.9892	0.9745	0.9820	A1
D_{BA}	0.8000	0.7667	0.8000	Undetermined	0.9700	0.9700	0.9700	Undetermined
S_F	0.1929	0.0251	0.0232	A1	0.9949	0.9927	0.3288	A1
S_{CCL}	0.7822	0.7667	0.7700	A1	0.9700	0.9700	0.9700	Undetermined
S_{GK}	0.6100	0.6044	0.6156	A3	0.9436	0.9428	0.9422	A1
D_{Hm}	0.5667	0.5444	0.5667	Undetermined	0.9700	0.9700	0.9700	Undetermined
S_{JJ}	0.6863	0.7554	0.7404	A2	0.9679	0.9665	0.9672	A1
D_{AS}^{P}	0.0998	0.1190	0.1266	A3	0.9833	0.9636	0.9724	A1
S_{LJ}	0.6170	0.5705	0.5761	A1	0.9821	0.9796	0.9811	A1

($p = 1$ in S_{DC}, S_{LS}^{E}, S_{LS}^{S}, S_{LS}^{H}, S_M and D_{BA}; $t = 2$ in D_{BA}; $\omega_i = 1/3$ in S_{LS}^{H})

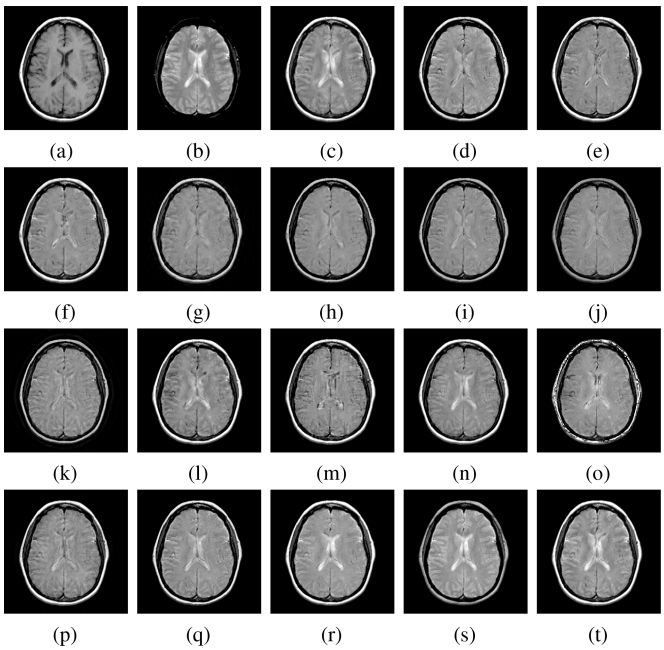

Fig. 9. The first set of fused medical images S1. (a) Image A; (b) Image B; (c) MSTBM; (d) MGIVF; (e) GFS; (f) CBF; (g) DCHWT; (h) ASR; (i) CSR; (j) MSVD; (k) CVT; (l) LP-SR; (m) RP-SR; (n) DWT-SR; (o) DTCWT-SR; (p) CVT-SR; (q) IFCNN; (r)SwinFusion; (s) EMFusion; (t) Our.

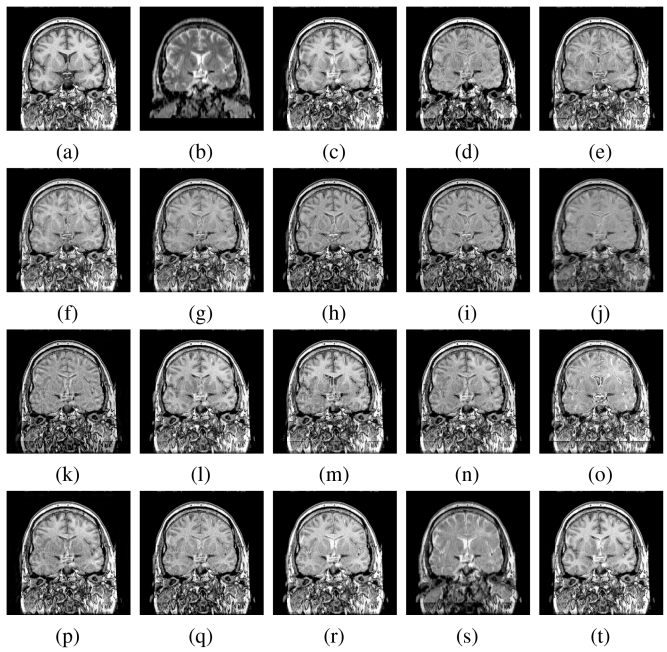

Fig. 10. The second set of fused medical images S2. (a) Image A; (b) Image B; (c) MSTBM; (d) MGIVF; (e) GFS; (f) CBF; (g) DCHWT; (h) ASR; (i) CSR; (j) MSVD; (k) CVT; (l) LP-SR; (m) RP-SR; (n) DWT-SR; (o) DTCWT-SR; (p) CVT-SR; (q) IFCNN; (r)SwinFusion; (s) EMFusion; (t) Our.

decision results with other similarities, such as S_{GK}, S_{JJ} and D_{AS}^{P} in Case 1. From the Table V, we can see that most of the existing measures do not make effective decision in these two cases, and our proposed measure S_{LJ} can make a reasonable decision according to the largest similarity value, and it can produce satisfactory performance.

From above experiments, it can be considered that our measure can make the rational decisions and achieve better effect compared with the contrastive measures in pattern recognition experiments. Thus, we can employ the proposed measure of IFSs for medical image fusion, and the following sub-section introduces the experiments on medical image fusion to verify the performance.

3) Example of Medical Image Fusion: We copy some real pixel values from the medical images to show the processes of our image fusion method, which are correspondence to the scheme in Fig. 2. In this example of medical image fusion, Fig. 8(a) presents the source images and the approximate position of the selected pixels, Fig. 8(b) presents the selected coefficients in the first layer in LPD, Fig. 8(c) presents membership degrees of the selected LPD coefficients, Fig. 8(d) presents the

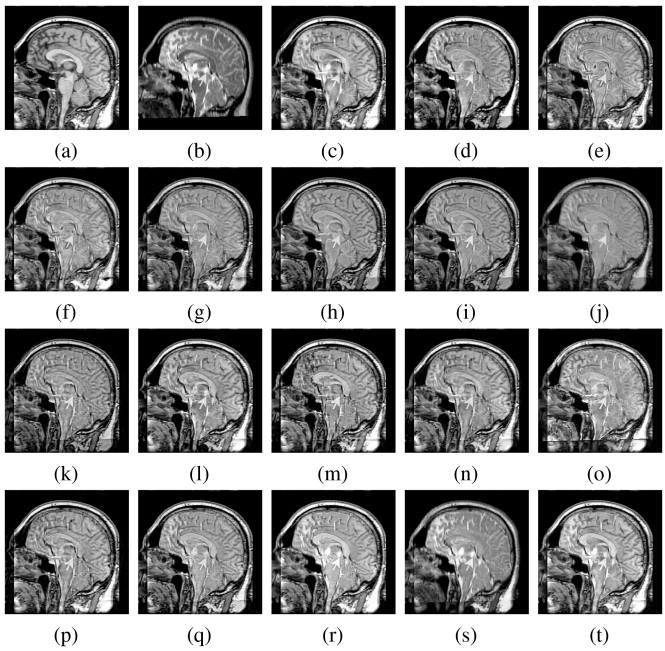

Fig. 11. The third set of fused medical images S3. (a) Image A; (b) Image B; (c) MSTBM; (d) MGIVF; (e) GFS; (f) CBF; (g) DCHWT; (h) ASR; (i) CSR; (j) MSVD; (k) CVT; (l) LP-SR; (m) RP-SR; (n) DWT-SR; (o) DTCWT-SR; (p) CVT-SR; (q) IFCNN; (r)SwinFusion; (s) EMFusion; (t) Our.

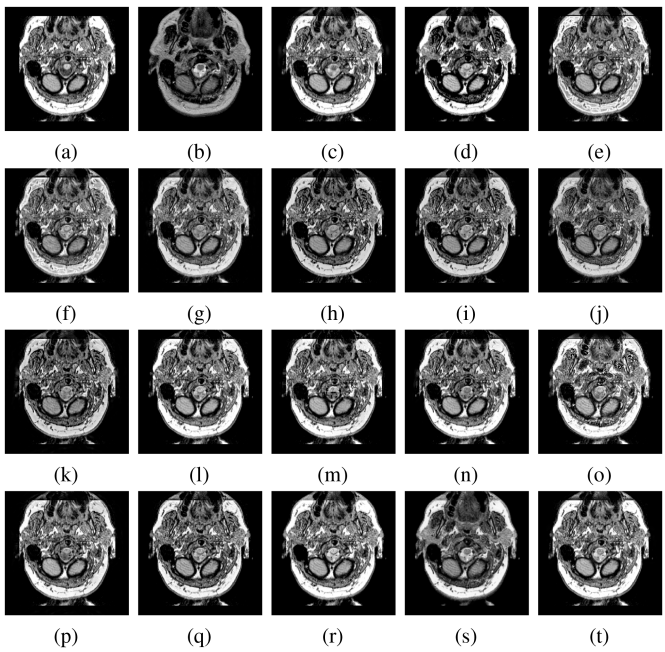

Fig. 12. The fourth set of fused medical images S4. (a) Image A; (b) Image B; (c) MSTBM; (d) MGIVF; (e) GFS; (f) CBF; (g) DCHWT; (h) ASR; (i) CSR; (j) MSVD; (k) CVT; (l) LP-SR; (m) RP-SR; (n) DWT-SR; (o) DTCWT-SR; (p) CVT-SR; (q) IFCNN; (r)SwinFusion; (s) EMFusion; (t) Our.

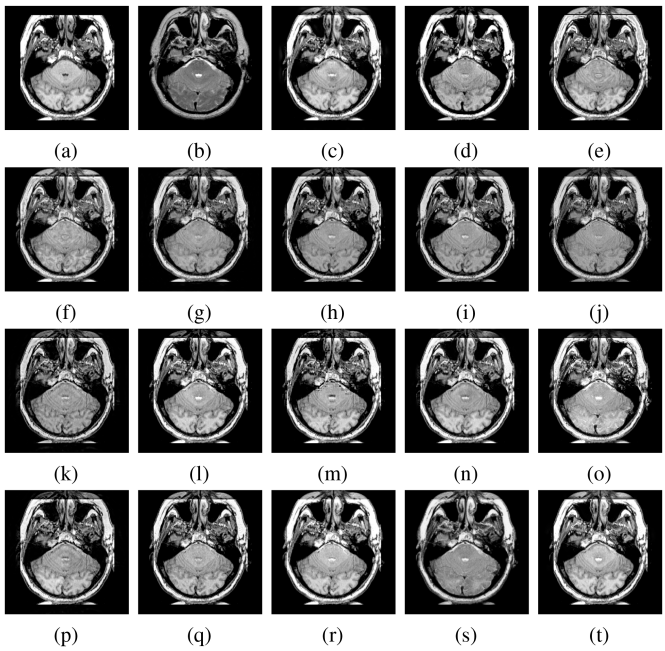

Fig. 13. The fifth set of fused medical images S5. (a) Image A; (b) Image B; (c) MSTBM; (d) MGIVF; (e) GFS; (f) CBF; (g) DCHWT; (h) ASR; (i) CSR; (j) MSVD; (k) CVT; (l) LP-SR; (m) RP-SR; (n) DWT-SR; (o) DTCWT-SR; (p) CVT-SR; (q) IFCNN; (r)SwinFusion; (s) EMFusion; (t) Our.

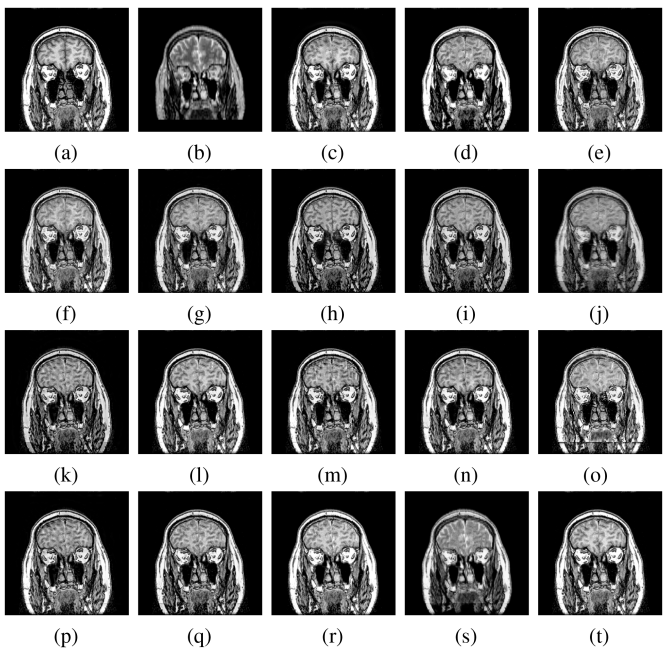

Fig. 14. The sixth set of fused medical images S6. (a) Image A; (b) Image B; (c) MSTBM; (d) MGIVF; (e) GFS; (f) CBF; (g) DCHWT; (h) ASR; (i) CSR; (j) MSVD; (k) CVT; (l) LP-SR; (m) RP-SR; (n) DWT-SR; (o) DTCWT-SR; (p) CVT-SR; (q) IFCNN; (r)SwinFusion; (s) EMFusion; (t) Our.

μ_{IFS}, ν_{IFS}, and π_{IFS} of the IFSs generated by the membership degrees, Fig. 8(e) presents the first similarity between the IFS (A and B) and the crisp IFS C, Fig. 8(f) presents the convolutional similarity matrix of Fig. 8(e) and 8(g) presents the fusion decisions, in which "0" means the pixel is abandoned and "1" means the pixel is retained. In this example, we can find the pixel values from the source image A are all bigger than these from source image B, but our fusion decisions for the pixels of source image A are different, which reveals that our method can make decision according to the source image pixels but not only

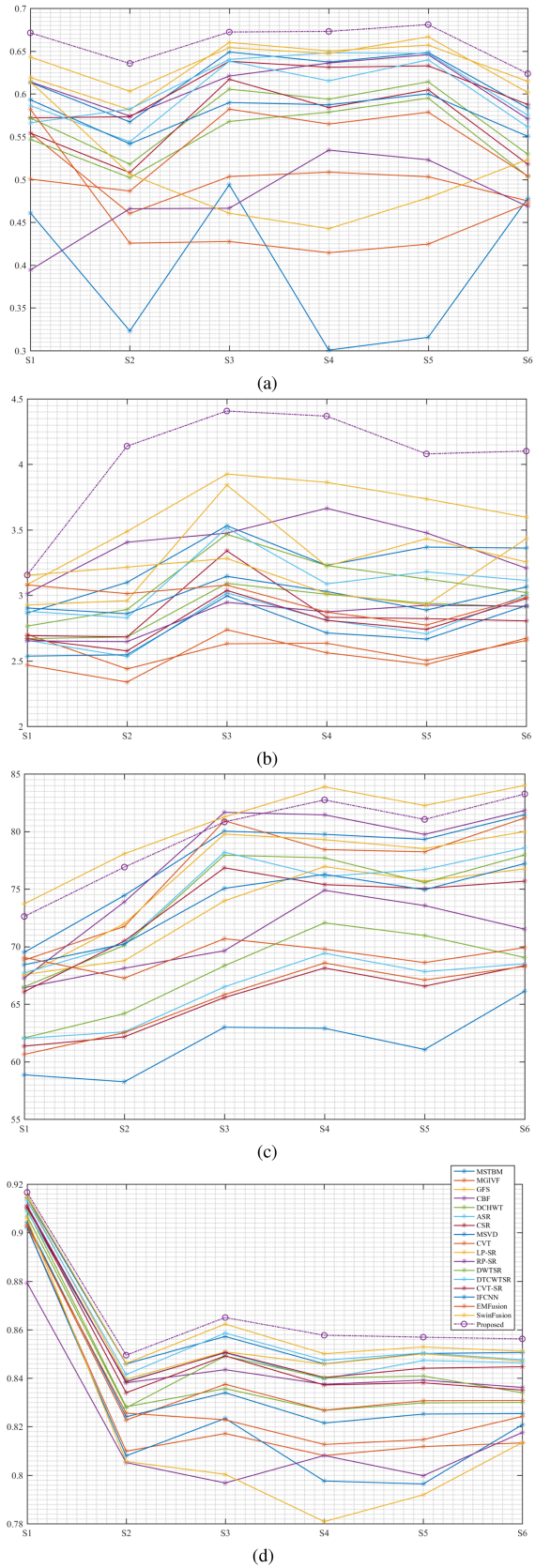

Fig. 15. Plots of objective indicators. (a) Q^{abf}; (b) MI; (c) STD; (d) FMI.

depend on it. Thus, we can infer that other useful information is taken into account, which indirectly verifies the effect of the proposed method.

B. Experiments of Medical Image Fusion

To learn the effectiveness of our proposed medical fusion image scheme on the basis of similar measure of IFSs, several popular fusion methods are performed to contrast with our new method, including MSTBM [6], MGIVF [39], GFS [40], CBF [41], DCHWT [42], ASR [43], CSR [44], MSVD [45], CVT [46], [47], LP-SR [47], RP-SR [47], DWT-SR [47], DTCWT-SR [47], CVT-SR [47], IFCNN [48], SwinFusion [49], and EMFusion [50].

In medical image fusion, edge based on similarity measure (Q^{abf}), mutual information (MI), standard deviation (STD), and feature mutual information (FMI) are the widely used evaluation metrics, which can be employed to verify the performance of fusion methods. Q^{abf} is used to evaluate edge information kept by the fused image. MI calculates the information quantity kept by the fused image. STD presents contrasting features of the final images with the statistical distribution. FMI shows the feature quantity of fused image obtaining from the source images.

Fig. 9 shows the first set of fused images generated by our method and other contrast fusion methods. Fig. 9 shows that most image fusion methods cannot effectively fuse the source images, but MSTBM, SwinFusion and our method can achieve outstanding performance as shown in Fig. 9(c), (r), and (t). Meanwhile, the brightness of some fused images, such as those in Fig. 9(i) and (j), are visibly inferior to that of other methods. In addition, the clarity of Fig. 9(m) and (n) suffers drops at different degrees. Thus, the effect of our method is superior to most of the contrast methods visually.

Fig. 10 presents the second set of fused medical images produced by different fusion methods. From Fig. 10, we can see that only four methods can effectively accomplish the fusion task of different medical images, such as MSTBM, RP-SR, SwinFusion, and the proposed method, and the corresponding fused images are shown in Fig. 10(c), (m), (r), and (t). Moreover, the brightness of some fused images, such as those in Fig. 10(i) and (j), are darker than other fused images. Besides, the clarity of Fig. 10(n) and (s) has the problem of the visibility declines.

Fig. 11 presents the third set of fused medical images produced by our method and the contrast fusion methods. The fused images in Fig. 11(c), (q), (r), and (t), which are generated by MSTBM, IFCNN, SwinFusion, and our proposed method, can accurately present the significant medical images features, but other methods cannot achieve good performance for the third pair of images. Meanwhile, the brightness of some fused images, such as those in Fig. 11(i), (j), and (s), are visibly inferior to that of other methods. In addition, the clarity of Fig. 11(n) is decreased.

The fourth set of fused medical images produced via our method and the contrast image fusion methods are shown in

TABLE VI
THE RUNTIME OF DIFFERENT METHODS (THE BEST RESULT ARE HIGHLIGHTED BY BOLD TYPE)

MSTBM	MGIVF	GFS	CBF	DCHWT	ASR	CSR	MSVD	CVT	LP-SR	RP-SR	DWT-SR	DTCWT-SR	CVT-SR	IFCNN	SwinFusion	EMFusion	Our
3.2557	0.082	3.694	4.3365	1.3428	70.8134	43.8651	0.1446	0.5318	0.2452	0.2647	0.3334	1.2788	0.9512	–	–	–	**0.0538**

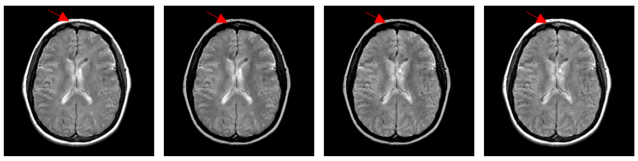

(a) (b) (c) (d)

Fig. 16. Ablation studies for fusion rules. (a) first combination of fusion rules; (b) second combination of fusion rules; (c) third combination of fusion rules; (d) fourth combination of fusion rules.

Fig. 12. We can see that most fusion methods do not get satisfying performance, and the fused images do not simultaneously present the features of the two medical images, except the fused images in Fig. 12(c), (r), and (t), which are generated by MSTBM, SwinFusion, and our method. Meanwhile, the brightness of some fused images, such as those in Fig. 12(h), (i), (j), and (k) generated by ASR, CSR, MSVD and CVT, are lower than that of other methods. In addition, the clarity of Fig. 12(n) is decreased.

Fig. 13 presents the fifth set of fused images produced by different image fusion methods. From Fig. 12, it can be seen that only the generated images in Fig. 13(c), (l), (m), (r) and (t) have the common characteristic of the medical images, and other methods cannot effectively fuse them. Furthermore, the brightness of some fused images are lower than that of other methods, such as the fused medical image in Fig. 13(h), (i), (j), and (k) which are respectively generated by ASR, CSR, MSVD, and CVT. In addition, the clarity of Fig. 13(m) and (n) suffers decrease to different degrees.

Fig. 14 is the fused results produced by different methods. We can see that the fusion performance of DCHWT, ASR, MSVD and RP-SR methods, which are shown in Fig. 14(g), (h),(j), (m) and (s), are poorer than other methods. Besides, the brightness of the generated images in Fig. 14(g), (h), (i), (j), and (k) generated by DCHWT, ASR, CSR, MSVD, and CVT are lower than that of other methods. Furthermore, the clarity of Fig. 14(j) and (n) suffers decrease to some degrees. Therefore, our proposed method is relatively superior to other image fusion methods, and it can be regarded as an excellent medical image fusion method subjectively.

Table VI shows the runtime of different fusion methods, which are calculated by averaging the time of ten times experiments, and we do not provide the running time of deep learning-based methods because the difference in the operating environment. In Table VI, we can find that the runtime of our method is the least. The runtime of our new method is similar to that of MGIVF. Besides, the runtime of MSVD, CVT, LP-SR, RP-SR, and DWT-SR are several times of the proposed method, and the runtime of MSTBM, GFS, CBF, DCHWT, and DTCWT-SR are dozens of times of our proposed method. In addition, the runtime of ASR and CSR are much more than that of the proposed method. Therefore, it can be concluded that the computation complexity of our new method is much less than that of other methods.

TABLE VII
OBJECTIVE INDICATORS OF FOUR DIFFERENT COMBINATIONS OF FUSION RULES

No.	High frequency	Low frequency	Qabf	MI	STD	FMI
1	Rule 1	Rule 2	0.6714	3.1553	72.6138	0.9166
2	Rule 1	Rule 1	0.5803	2.9061	65.8989	0.9036
3	Rule 2	Rule 1	0.5324	2.6508	67.5079	0.9005
4	Rule 2	Rule 2	0.6201	2.9980	74.0829	0.9138

The plots of objective indicators of different methods are displayed in Fig. 15, in which we can see that the curves of our proposed medical image fusion method are better than most of other fusion methods. The scores of mathematical indicators of different fusion methods are provided in Supplementary Materials. For the frequently-used indicators of image fusion, MI and Q^{abf} are the most significant two indicators, because they can measure the difference between the fused image and the corresponding source medical images. Fig. 15 shows that the scores of our method are higher than those of the competitors in terms of MI, Q^{abf}, and FMI values, which reveals that our new method can present and fuse more features from the source medical images compared with these contrast methods. In addition, the STD score of our proposed method are superior to most of other methods, except EMFusion and RP-SR (only the third experiments). But the STD value of our method is still competitive to other methods. In summary, the evaluation indexes reveal that our new proposed medical fusion method using the new fuzzy similarity measure between IFSs is superior to most competitors.

C. Ablation Studies

We performed four ablation studies to show the effectiveness of our image fusion rules. The results are shown in Table VII and Fig. 16, we can find that the three scores of No. 1 combination are the best, and the visual effect of No. 1 are also competitive, such as the position marked by the red arrow. The experiments show that our used combination (No. 1) achieved better performance in terms of objective and subjective index indicators.

V. CONCLUSION

This work proposes an effective similarity measure between IFSs by introducing geometric modeling technique, and a lightweight medical image fusion method is also designed according to the new measure. First, a new similarity measure of IFS theory is conducted to improve the performance. Second, our new measure is applied to represent the medical image features of the obtained sub-band images which are decomposed by LPD. Third, two fusion rules are used to integrate the decomposed sub-band images. At last, the final result is recovered by reverse

LPD. The experiments show that our similarity measure is reasonable and effective, and the performance of our proposed method is more effective than that of the contrast fusion methods with smaller cost.

This study combines the fuzzy measure of IFSs with multi-scale image analysis technique to describe and extract the imprecise features of medical images, so that the fused pixels can be determined based on the measured similarity information, which reveals the effectiveness of the similarity measure between IFSs in medical image fusion. In this work, our proposed similarity measure between IFSs can overcome the shortcomings of most existing theoretical models to provide reasonable decisions. Besides, this work also further expands the real application of similarity measure between IFSs and provides an effectively theoretical tools for medical image fusion.

ACKNOWLEDGMENT

The authors thank the editors and the anonymous reviewers for their careful works and valuable suggestions for this study. The authors thank Oliver R. for his kindly sharing of Pixel-Level Image Fusion and the Image Fusion Toolbox that is available at http://www.metapix.de/toolbox.htm.

REFERENCES

[1] L. A. Zadeh, "Fuzzy sets," *Inf. Control*, vol. 8, no. 3, pp. 338–353, 1965.
[2] M. Das and S. K. Ghosh, "Reducing parameter value uncertainty indiscrete Bayesian network learning: A semantic fuzzy Bayesian approach," *IEEE Trans. Emerg. Topics Comput. Intell.*, vol. 5, no. 3, pp. 361–372, Jun. 2021.
[3] L. Li, L. Jiang, C. Bu, Y. Zhu, and X. Wu, "Interval-valued intuitionistic fuzzy decision with graph pattern in big graph," *IEEE Trans. Emerg. Topics Comput. Intell.*, vol. 6, no. 5, pp. 1057–1067, Oct. 2022.
[4] L. Ghosh, A. Konar, P. Rakshit, and A. K. Nagar, "Hemodynamic analysis for cognitive load assessment and classification in motor learning tasks using Type-2 fuzzy sets," *IEEE Trans. Emerg. Topics Comput. Intell.*, vol. 3, no. 3, pp. 245–260, Jun. 2019.
[5] T. Sharma and N. K. Verma, "Estimating depth and global atmospheric light for image dehazing using Type-2 fuzzy approach," *IEEE Trans. Emerg. Topics Comput. Intell.*, vol. 6, no. 1, pp. 93–102, Feb. 2022.
[6] Z. Zhu, M. Zheng, G. Qi, D. Wang, and Y. Xiang, "A Phase congruency and local Laplacian energy based multi-modality medical image fusion method in NSCT domain," *IEEE Access*, vol. 7, pp. 20811–20824, 2019.
[7] K. Kolomvatsos, "Data-driven Type-2 fuzzy sets for tasks management at the edge," *IEEE Trans. Emerg. Topics Comput. Intell.*, vol. 6, no. 2, pp. 377–386, Apr. 2022.
[8] L. A. Zadeh, "The concept of a linguistic variable and its application to approximate reasoning- I," *Inf. Sci.*, vol. 8, no. 3, pp. 199–249, 1975.
[9] K. Atanassov, "Intuitionistic fuzzy sets," *Fuzzy Sets Syst.*, vol. 20, pp. 87–96, 1986.
[10] S. M. Chen, "Measures of similarity between vague sets," *Fuzzy Sets and Syst.*, vol. 74, no. 2, pp. 217–223, 1995.
[11] S. M. Chen, S. H. Cheng, and T. C. Lan, "A novel similarity measure between intuitionistic fuzzy sets based on the centroid points of transformed fuzzy numbers with applications to pattern recognition," *Inf. Sci.*, vol. 343, pp. 15–40, 2016.
[12] W. Hung and M. Yang, "Similarity measures of intuitionistic fuzzy sets based on Lp metric," *Int. J. Approx. Reasoning*, vol. 46, no. 2007, pp. 120–136, 2007.
[13] J. Ye, "Cosine similarity measures for intuitionistic fuzzy sets and their applications," *Math. Comp. Modelling*, vol. 53, no. 2011, pp. 91–97, 2011.
[14] H. Nguyen, "A novel similarity/dissimilarity measure for intuitionistic fuzzy sets and its application in pattern recognition," *Expert Syst. Appl.*, vol. 45, no. C, pp. 97–107, 2016.
[15] K. He, J. Gong, L. Xie, X. Zhang, and D. Xu, "Regions preserving edge enhancement for multisensor-based medical image fusion," *IEEE Trans. Instrum. Meas.*, vol. 70, 2021, Art. no. 5008513.
[16] X. Li, X. Guo, P. Han, X. Wang, H. Li, and T. Luo, "Laplacian redecomposition for multimodal medical image fusion," *IEEE Trans. Instrum. Meas.*,, vol. 69, no. 9, pp. 6880–6890, Sep. 2020.
[17] Jin X. Jiang et al., "Brain medical image fusion using L2-Norm-Based features and fuzzy-weighted measurements in 2D littlewood-paley EWT domain," *IEEE Trans. Instrum. Meas.*, vol. 69, no. 9, pp. 5900–5913, Aug. 2020.
[18] G. Bhatnagar, Q. M. J. Wu, and Z. Liu, "Directive contrast based multimodal medical image fusion in NSCT domain," *IEEE Trans. Multimedia*, vol. 15 no. 5, pp. 1014–1024, Aug. 2013.
[19] H. Xu, J. Ma, J. Jiang, X. Guo, and H. Ling, "U2Fusion: A unified unsupervised image fusion network," *IEEE Trans. Pattern Anal. Mach. Intell.*, vol. 44, no. 1, pp. 502–518, Jan. 2022.
[20] L. De Miguel et al., "Construction of admissible linear orders for interval-valued Atanassov intuitionistic fuzzy sets with an application to decision making," *Inf. Fusion*, vol. vol. 27, pp. 189–197, 2016.
[21] H. Bustince et al., "Similarity between interval-valued fuzzy sets taking into account the width of the intervals and admissible orders," *Fuzzy Sets Syst.*, vol. 390, pp. 23–47, 2020.
[22] J. M. Mendel, H. Hagras, H. Bustince, and F. Herrera, "Comments on interval Type-2 fuzzy sets are generalization of interval-valued fuzzy sets: Towards a wide view on their relationship," *IEEE Trans. Fuzzy Syst.*, vol. 24, no. 1, pp. 249–250, Feb. 2016.
[23] K. Atanassov and G. Gargov, "Interval-valued intuitionistic fuzzy sets," *Fuzzy Sets Syst.*, vol. 31, pp. 343–349, 1989.
[24] K. Atanassov, "Intuitionistic fuzzy sets," *Fuzzy sets Syst.*, vol. 20, pp. 87–96, 1986.
[25] L. Dengfeng and C. Chuntian, "New similarity measures of intuitionistic fuzzy sets and application to pattern recognitions," *Pattern Recognit. Lett.*, vol. 23, pp. 221–226, 2002.
[26] E. Szmidt and J. Kacprzyk, "A similarity measure for intuitionistic fuzzy sets and its application in supporting medical diagnostic reasoning," *Lecture Notes Artif. Intell.*, vol. 3070, pp. 388–393, 2004.
[27] E. Szmidt and J. A. Kacprzyk, "New similarity measure for intuitionistic fuzzy sets: Straightforward approaches may not work," in *Proc. IEEE Int. Fuzzy Syst. Conf.*, 2007, pp. 1–4.
[28] A. F. Santiago, H. C. Ariel, and V. S F. Gonzalo, "A local fuzzy thresholding methodology for multiregion image segmentation," *Knowl.-Based Syst.*, vol. 83, pp. 1–12, 2015.
[29] S. M. Chen, "Measures of similarity between vague sets," *Fuzzy Sets Syst.*, vol. 74, pp. 217–223, 1995.
[30] D. H. Hong and C. A. Kim, "A note on similarity measures between vague sets and between elements," *Inf. Sci.*, vol. 115, no. 1999, pp. 83–96, 1999.
[31] Z. Liang and P. Shi, "Similarity measures on intuitionistic fuzzy sets," *Pattern Recognit. Lett.*, vol. 24, no. 2003, pp. 2687–2693, 2003.
[32] H. B. Mitchell, "On the Dengfeng Chuntian similarity measure and its application to pattern recognition," *Pattern Recognit. Lett.*, vol. 24, no. 2003, pp. 3101–3104, 2003.
[33] W. Wang and X. Xin, "Distance measure between intuitionistic fuzzy sets," *Pattern Recognit. Lett.*, vol. 26, pp. 2063–2069, 2005.
[34] F. E. Boran and D. A. Akay, "A biparametric similarity measure on intuitionistic fuzzy sets with applications to pattern recognition," *Inf. Sci.*, vol. 255, pp. 45–57, 2014.
[35] R. T. Ngan et al., "H-max distance measure of intuitionistic fuzzy sets indecision making," *Appl. Soft Comput.*, vol. 69, pp. 393–425, 2018, Art. no. 2018b.
[36] H. Garg and K. Kumar, "An advanced study on the similarity measures of intuitionistic fuzzy sets based on the set pair analysis theory and their application in decision making," *Soft Comput.*, vol. 22, no. 15, pp. 4959–4970, 2018.
[37] Q. Jiang, X. Jin, and S. J. Lee, "A new similarity/distance measure between intuitionistic fuzzy sets based on the transformed isosceles triangles and its applications to pattern recognition," *Expert Syst. with Appl.*, vol. 116, pp. 439–453, 2019.
[38] A. Singh and S. A. Kumar, "novel dice similarity measure for IFSs and its applications in pattern and face recognition," *Expert Syst. with Appl.*, vol. 149, 2020, Art. no. 113245.
[39] D. P. Bavirisetti et al., "Multi-scale Guided Image and Video Fusion: A Fast and Efficient Approach," *Circuits, Syst., Signal Process.*, vol. 38, no. 12, pp. 5576–5605, 2019.
[40] D. P. Bavirisetti et al., "Fusion of MRI and CT images using guided image filter and image statistics," *Int. J. Imag. Syst. Technol.*, vol. 27, no. 3, pp. 227–237, 2017.
[41] B. K. S. Kumar, "Image fusion based on pixel significance using cross bilateral filter," *Signal Image Video Process.*, vol. 9, no. 5, pp. 1193–1204, 2015.

[42] B. K. S. Kumar, "Multifocus and multispectral image fusion based on pixel significance using discrete cosine harmonic wavelet transform," *Signal Image Video Process.*, vol. 7, no. 6, pp. 1125–1143, 2013.
[43] Y. Liu and Z. Wang, "Simultaneous image fusion and denoising with adaptive sparse representation," *IET Image Process.*, vol. 9, no. 5, pp. 347–357, 2014.
[44] Y. Liu, X. Chen, R. K. Ward, and Z. Jane Wang, "Image fusion with convolutional sparse representation," *IEEE Signal Process. Lett.*, vol. 23, no. 12, pp. 1882–1886, Dec. 2016.
[45] V. P. S. Naidu, "Image fusion technique using multi-resolution singular value decomposition," *Defence Sci. J.*, vol. 61, no. 5, pp. 479–484, 2011.
[46] E. Candes et al., "Fast discrete curvelet transforms," *Multiscale Model. Simul.*, vol. 5, no. 3, pp. 861–899, 2006.
[47] Y. Liu, S. Liu, and Z. Wang, "A general framework for image fusion based on multi-scale transform and sparse representation," *Inf. Fusion*, vol. 24, pp. 147–164, 2015.
[48] Y. Zhang et al., "IFCNN: A general image fusion framework based on convolutional neural network," *Inf. Fusion*, vol. 54, pp. 99–118, 2020.
[49] H. Xu and J. Ma, "EMFusion: An unsupervised enhanced medical image fusion network," *Inf. Fusion*, vol. 76, pp. 177–186, 2021.
[50] J. Ma, L. Tang, F. Fan, J. Huang, X. Mei, and Y. Ma, "SwinFusion: Cross-domain long-range learning for general image fusion via swin transformer," *IEEE/CAA J. Autom. Sinica*,, vol. 9, no. 7, pp. 1200–1217, Jul. 2022.

Qian Jiang received the B.S. degree in thermal energy and power engineering and the M.S. degree in power engineering and engineering thermophysics from Central South University, Changsha, China, in 2012 and 2015, respectively, and the Ph.D. degree in communication and information systems from Yunnan University, Kunming, China, in 2019. She is currently an Associate Professor with the School of Software, Yunnan University. Her research interests include deep neural networks, fuzzy set theory, bio-informatics, image processing, and information fusion.

Xin Jin (Member, IEEE) received the B.S. degree in electronics and information engineering from Henan Normal University, Xinxiang, China, in 2013, and the Ph.D. degree in communication and information systems from Yunnan University, Kunming, China, in 2018. He is currently an Associate Professor with the School of Software, Yunnan University. His research interests include neural networks, image processing, information fusion, optimization algorithm, and fuzzy set theory.

Xiaohui Cui received the Ph.D. degree in computer science and engineering from the University of Louisville, Louisville, KY, USA, in 2004. He is currently a Professor with the School of Cyber Science and Engineering, Wuhan University, Wuhan, China. His main research interests include Big Data, cluster intelligence theory, blockchain technology, image processing, food safety, and high-performance computing.

Shaowen Yao (Member, IEEE) received the B.S. and M.S. degrees in telecommunication engineering from the Yunnan University, Kunming, China, in 1988 and 1991, respectively, and the Ph.D. degree in computer application technology from the University of Electronic Science and Technology of China, Chengdu, China, in 2002. He is currently a Professor with the School of Software, Yunnan University. His research interests include neural networks, fuzzy set theory, image processing, bio-informatics, and data mining.

Keqin Li (Fellow, IEEE) is currently a SUNY Distinguished Professor of computer science with the State University of New York, Albany, NY, USA. He is also a National Distinguished Professor with Hunan University, Changsha, China. He has authored or coauthored more than 870 journal articles, book chapters, and refereed conference papers. He holds nearly 70 patents announced or authorized by the Chinese National Intellectual Property Administration. His research interests include cloud computing, fog computing and mobile edge computing, energy-efficient computing and communication, embedded systems and cyber-physical systems, heterogeneous computing systems, Big Data computing, highperformance computing, CPU-GPU hybrid and cooperative computing, computer architectures and systems, computer networking, machine learning, and intelligent and soft computing. He was the recipient of several best paper awards. He is among the worlds top five most influential scientists in parallel and distributed computing in terms of both single-year impact and career-long impact based on a composite indicator of Scopus citation database. He has chaired many international conferences. He is currently an Associate Editor for the *ACM Computing Surveys* and *CCF Transactions on High Performance Computing*. He has served on the Editorial Boards of the IEEE TRANSACTIONS ON PARALLEL AND DISTRIBUTED SYSTEMS, IEEE TRANSACTIONS ON COMPUTERS, IEEE TRANSACTIONS ON CLOUD COMPUTING, IEEE TRANSACTIONS ON SERVICES COMPUTING, and IEEE TRANSACTIONS ON SUSTAINABLE COMPUTING. He is an AAIA Fellow. He is also a Member of Academia Europaea (Academician of the Academy of Europe).

Wei Zhou (Member, IEEE)received the Ph.D. degree from the University of Chinese Academy of Science, Beijing, China, in 2008. He is currently a Full Professor with the School of Software, Yunnan University, Kunming, China. His research interests include distributed data intensive computing, image processing, bio-informatics, neural networks, and information security.